

Petrographic and Diagenetic Characteristics of Banded Iron-Formation (BIF): A Case Study of The Kuruman Formation (Transvaal Supergroup) in the Prieska Area, Northern Cape Province, South Africa

Mainly Abongile Mbongonya¹, Kuiwu Liu¹, and Christopher Baiyegunhi²

¹ Department of Geology, University of Fort Hare, Private Bag X1314, Alice 5700, Eastern Cape Province, South Africa

² Department of Geology and Mining, University of Limpopo, Private Bag X1106, Sovenga 0727, Limpopo Province, South Africa

Received November 14, 2022; Accepted May 26, 2023

Abstract

The Kuruman Formation in the Transvaal Supergroup, Northern Cape Province of South Africa, contains several iron and manganese ore deposits, resulting in numerous studies, particularly within the northern Ghaap plateau compartment where most iron and manganese mines are located. However, fewer studies have been conducted in the southern Prieska Compartment, especially on the origin and post-depositional alteration of the banded iron formation (BIF). Thus, the study is targeted at the Kuruman Formation in the Prieska area to investigate the diagenetic characteristics of the BIF using field observations, petrographic and geochemical methods. The studies revealed four mineral paragenetic groups constituting primary minerals, diagenetic minerals, low-grade metamorphic minerals, and weathering mineral assemblages were encountered in the area. Post-depositional mineral alteration studies show that most of the primary minerals have experienced various degrees of alteration. The bulk of silicate and iron oxide minerals have been recrystallized, partially replaced, dissolved, or leached out. Multiple formation processes were involved in the origin of the banded iron formation: (1) deposition of iron-rich mud material on the deep ocean floor, as well as the formation of an iron-rich mud mixture (felutite) on the seafloor; (2) Felutite differentiation and the formation of disseminated iron-oxide from mud; (3) Cohesion and diagenesis of disseminated iron-oxide and the formation of iron-rich (magnetite/hematite) and silica-rich (chert/quartz) patches, microbands, and laminations; (4) Consolidation and compaction, leading to the final banded iron formation (BIF).

Keywords: Petrography; Mineral paragenesis; Post-depositional alteration; Banded iron formation (BIF); Kuruman Formation; Prieska.

1. Introduction

Banded iron formations (BIFs) are well-known Precambrian iron-rich chemical sedimentary rocks, with peak deposition occurring [1-4]. These BIFs are distinguished by their alternating iron-rich iron oxide (magnetite, hematite) and iron-poor chert (quartz), with variable amounts of iron carbonates (siderite, ankerite) and iron silicates (greenalite, grunerite, etc.), meters (macro-bands), centimetres to micrometres (mesobands), and/or millimetres (microbands) [4-11]. The original BIF minerals may be challenging to identify due to the vulnerability of iron-rich minerals to changes in redox conditions, which can overprint paleoenvironmental and biological signatures during diagenesis, metamorphism, and weathering [12-13]. None of the BIF minerals are primary, but they rather reflect diagenetic, metamorphic, and weathering overprinting that results from the unstable precursor minerals that universally recrystallize to a more stable diagenetic, metamorphic, and supergene/weathering assemblage of dehydrated minerals [12,14].

The mineralogy of the unweathered BIF successions that experienced diagenesis to low-grade metamorphism is remarkably uniform, comprising mostly chert (SiO₂), magnetite

(Fe_3O_4), hematite (Fe_2O_3), iron carbonates (i.e., siderite, ankerite, dolomite, and calcite), and various iron–silicate minerals (i.e., greenalite, stilpnomelane, minnesotaite, and riebeckite) [15-17,19-20,37]. The post-depositional BIF mineralogy obscures the understanding of primary depositional mechanisms and makes the accurate interpretation of the key precipitation processes in BIFs difficult [15-20]. The post-depositional physicochemical modifications of the BIF have largely obliterated original textures and mineralogy and may be responsible for much of the micro-banding seen in these rocks. The economically viable BIF-derived major global direct-shipping iron-ore bodies are typically found within post-depositional lower greenschist to amphibolite facies tectono-metamorphic and deeply weathered regolith [21-23]. These iron ore deposits, which extend to considerable depths below low-grade goethitised surface horizons and the water table, showing well-preserved primary structures and textures, are widely considered to be derived from the BIFs by selective supergene leaching of the gangue minerals (i.e., chert, carbonates, and iron silicates) [22]. The BIF weathers rapidly within a few metres of the surface exposure, particularly when rich in ferrous carbonate and/or ferrous iron silicates, which is why the weathering/supergene enrichment of the BIF to low-grade ore is common in near-surface environments above the water table, such as ferruginised BIF outcrops, detrital ore deposits, and shallow ore deposits that have been subjected to prolonged exposure to fresh meteoric water [23]. The highly weathered BIF, which is usually characterised by friable chert bands, leached or goethitised oxide bands, and goethite pseudomorphs of iron silicates and carbonates, differs greatly from the unoxidised and unweathered BIF that typically contains ubiquitous iron silicates, carbonates, and apatite as minor constituents [23].

The BIFs have been extensively studied due to their economic importance, but many aspects of their post-depositional processes remain enigmatic because modern analogues are unknown. There is very little published information on the post-depositional alteration of low-grade BIFs; typically the weathering effects on the mineralogical composition of the BIFs, particularly in the Griqualand West basin of the Transvaal Supergroup. This paucity of information is in contrast to the comprehensive post-depositional data that is readily available for the protolith BIFs [16, 18, 24-26]. Compared to some of the better-studied BIFs, the Prieska BIF warrants more attention, particularly regarding the origin and post-depositional alteration of the banded iron formation (BIF). Therefore, this contribution gives insight into the effects of diagenesis on the mineralogical composition of banded iron-formation (BIF) of the Kuruman Formation in the Prieska area. This study draws attention to a generally neglected aspect of the petrography and diagenetic characteristics of these rocks, particularly since unsuspected alteration can give rise to misleading chemical data. Thus, it is meant to complement the discussion on the difficulties inherent in sampling banded iron-formation (BIF) to produce representative information.

2. Geological setting

The Prieska study area is covered by the Kuruman Formation of the Asbestos Hills Subgroup, hosted by the Ghaap Group of the Griqualand West sequence within the preserved Paleoproterozoic (2.7–2.2 Ga) Transvaal Supergroup [7], which covers approximately 250,000 km² of the Archaean Kaapvaal Craton (Figure 1) [15]. The Griqualand West Basin and its associated sequences, which are slightly deformed and metamorphosed below the zeolite grade, are located on the western margin of the Kaapvaal Craton in South Africa and are separated by the Vryburg Arch from the Transvaal sub-basin on the south-western rim of the Archaean Kaapvaal Craton [27-35]. The deformation is characterized by intense folding and faulting, which is more pronounced in the south-western margin (Kheis Province), adjacent to the Namaqualand Metamorphic Belt, and is delimited to the west by the sharp NW-SE trending tectonic Doringberg Fault System, which runs on its south-western termination [36-38]. The basal Ghaap Group of the Griqualand West sequence comprises a clastic and a relatively pure chemical sedimentary rock sequence that is unconformably overlain by a mixed siliciclastic-volcanic Postmasburg Group rock package and the Voelwater Subgroup's chemical sediments at the stratigraphic top [36-40]. The Griqualand West sub-basin is subdivided into the Ghaap Plateau and the Prieska compartments, separated by the NW-SE trending Griquatown Fault Zone

(GFZ) (Figure 1) and showing indistinguishable lithological successions of partly varying ages in their basal stratigraphic levels and contrasting mineral potential [34,37].

The transgressive Asbestos Hills Subgroup sediments are predominantly composed of the 1000 m thick, well-developed basal Kuruman and top Griquatown iron formation units that extend over 500 km north-south below the siliciclastic rocks of the Koegas Subgroup and conformably cover the Campbellrand Subgroup carbonate rocks [36-38]. The rhythmically micro-banded Kuruman and the overlying Griquatown Iron Formations are challenging to separate geochemically, and they comprise cherty layers enriched in blue riebeckite and brown to black stilpnomelane bands on fresh outcrops intercalated in the BIF sequence [29, 37]. These iron formations grade upwards into the Koegas Subgroup within the Prieska sub-basin and have been greatly impacted by thrust faults in the south of the Griquatown Fault zone [36]. The fault movements that mainly affected the BIFs because of the incompetency of some of their beds and their laminated characters were directed east, north-east, and south-east. Within these iron formations, shale horizons separate the individual BIF macro-bands, which are further subdivided into meso- and microbands dominated by iron oxide minerals (i.e., magnetite, hematite), iron silicates, and iron carbonates, alternating with bands dominated by chert (i.e., microcrystalline quartz) [11].

The Superior-type Kuruman Formation is an autochthonous, variable (210 m) thick Precambrian cherty iron formation (IF) that is chemically continuous over hundreds of kilometers, formed on a continental platform separated by Naute Shale and consisting primarily of pelites and a few intercalated cherts from the Campbellrand Subgroup in the Prieska-Koegas area to the south [44]. The formation was subjected to very low-grade metamorphism and is composed primarily of fine-grained mudrock, chert, and iron minerals (siderite, magnetite, and hematite) that grade upward through the stratigraphy, becoming more granular chert-carbonate-magnetite BIF [27-29, 42-45]. The Kuruman Formation is cross-cut by two basaltic andesitic sills, with the BIFs immediately around these sills depleted in carbonate due to contact metamorphism. The IF is divided into the Kliphuis Member at the base, the Groenwater Member, Riries Member, and the Ouplass sedimentological member at the top, which are harder to distinguish at the carbonate platform top and in drill core sections [29, 42]. The study area is particularly covered by the lower Kliphuis and partially Groenwater members of the Kuruman Formation [29, 43]. The Kuruman BIF is highly deformed in the area, and it occurs with shale and claystone partings. The BIF is medium to fine-grained, exhibiting a typical banded texture and consists of iron bands with variegated grain size. The bands are nearly parallel to the alternated layers of iron minerals and silica (quartz).

3. Materials and methods

Fieldwork was carried out in the roadcut exposures of the Prieska banded iron formation in the Northern Cape Province, South Africa. Stratigraphic measurements were performed on four road-cut sections (1-4) along the national road N10 (Figure 1). A total of 66 thin sections of the 22 representative BIF samples collected from the study area (Figure 1) were studied under an optical microscope to determine their mineralogical compositions, textural characteristics, and cement types. Furthermore, 22 samples were cleaned, glued on a glass microscope slide and gold coated using a Cressington Gold Coater 108 Gold/A machine. The coated samples were analysed using a scanning electron microscopy (SEM) instrument (Model: JEOL JSM-6390LV) fitted with an energy dispersive x-ray microanalyser (EDX). The samples were observed in backscattered electron (BSE) and secondary electron imaging (SEI) modes of imaging. The cement types, textures, and primary and authigenic minerals of the sandstones were described based on petrographic studies of thin sections and SEM and EDX analyses. Furthermore, clay minerals, quartz overgrowth, diagenetic textures, dissolution effects, and other related diagenetic imprints were examined using SEM. In addition, 10 representative samples were also analysed by X-ray diffraction (XRD) to determine their mineral compositions. The XRD was performed using a standardized Panalytical back-loading system.

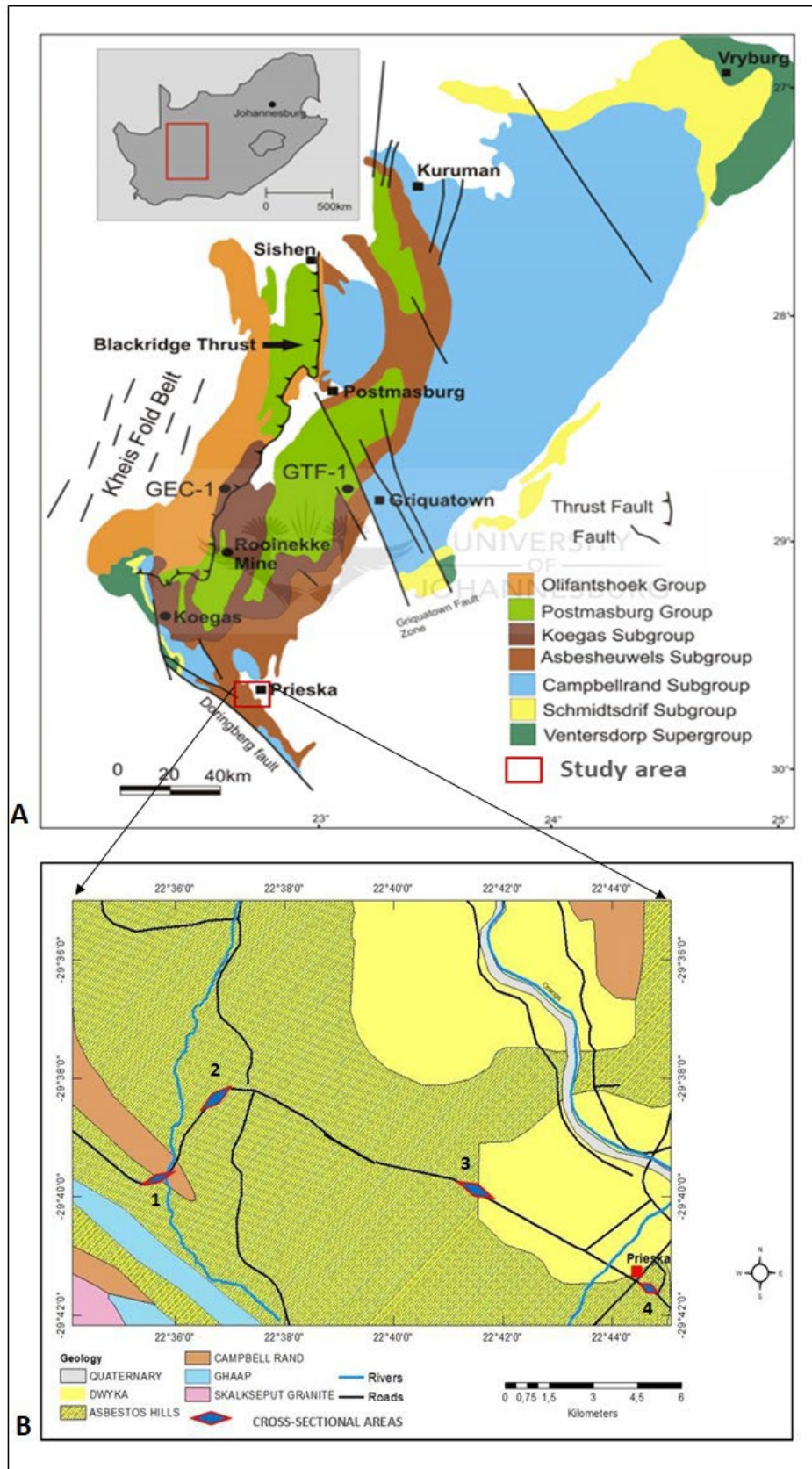


Figure 1. Geological map showing (A) stratigraphic and structural occurrences in the Griqualand West Basin [46]; (B) cross-sectional areas and local geology of the Prieska area

The XRD analysis was carried out using the standardized Panalytical back-loading system. The diffractograms were obtained by means of a PANalytical X'Pert Pro powder diffractometer with an X'Celerator detector and variable divergence and fixed receiving slits with Fe filtered Co-K α radiation ($\lambda=1.789\text{\AA}$). The phases were identified using X'Pert Highscore plus software, while the relative phase amounts (weight%) were estimated using the Rietveld method. It is important to note that mineral abundances below 1% remain undetectable by the powdered XRD method. In contrast, those between 1 and 5% exhibit minor spectra peaks, and their intensities are too low for accurate identification. Thus, approximate mineral abundances were inferred by integrating semi-qualitative XRD and petrographic methods such as SEM and optical microscopy.

4. Results and discussion

4.1. Field observations

The stratigraphic sections of the Prieska BIF in the study area are presented in the supplementary data (Figure 2-5). The mapped Kuruman Iron Formation comprises deformed and highly weathered BIF rocks that dip towards the south-east with fresher road cuts (Figure 6). The BIF consists of blackish to reddish-brown colour variations encountered in the different layers and sections. The formation contains dark to black layers of magnetite, hematite, and small varying concentrations of yellowish to orange goethite and limonite (Figure 6b). Chert (quartz), iron oxides, clay minerals, and carbonate layers are the dominant constituents within the Prieska BIF. The BIF is encountered with magnetite interlayered with hematite, goethite, chert, and carbonate-rich microbands (Figure 6f). The highly weathered zones are characterized by significant amounts of limonite and goethite (Figure 6g). There are openings (joints, faults, cracks, and bedding planes), some of which are filled with quartz and secondary calcrete. There is a variation in the BIF bands and laminations across the study area, with some bands being thicker than others. There are thin laminations of carbonate and silicates, iron, and chert. There is a transitional bed present from the thick to medium bedding dominated by hematite and goethite in some places. It comprises weathered magnetite laminations, hematite, and goethite laminations. Some of the BIF rocks have bands comprising a mixture of hematite and goethite. Some areas contain more hematite and goethite with less magnetite. There is a green tint that is associated with the chert and magnetite layers. The BIF is thin to medium-laminated with a dark colour that changes to brownish towards the north-west (top). The laminations increase to thin beds and back to medium laminations towards the younger side. Most BIF bands are hematite-rich, either as continuous bands, lenticulars, or pod structures. The other bands and laminations are rich in chert, while others are more magnetite-rich. The magnetite is exposed to the surface, and it changes to a reddish hematite. The BIF appears with calcrete on the surface due to leaching and evaporation. There is a huge fault that is evident in the area. The formation is highly weathered towards the north-west, with a huge fault evident in the area, and there is more calcrete visible towards the younger side. There are also some quartz veins visible. There are chert (greyish) layers interbedded with iron and mud-rich layers, some of which are about 1 to 5 cm thick (Figure 6i). Some of the chert layers are lenticular, while some are deformed.

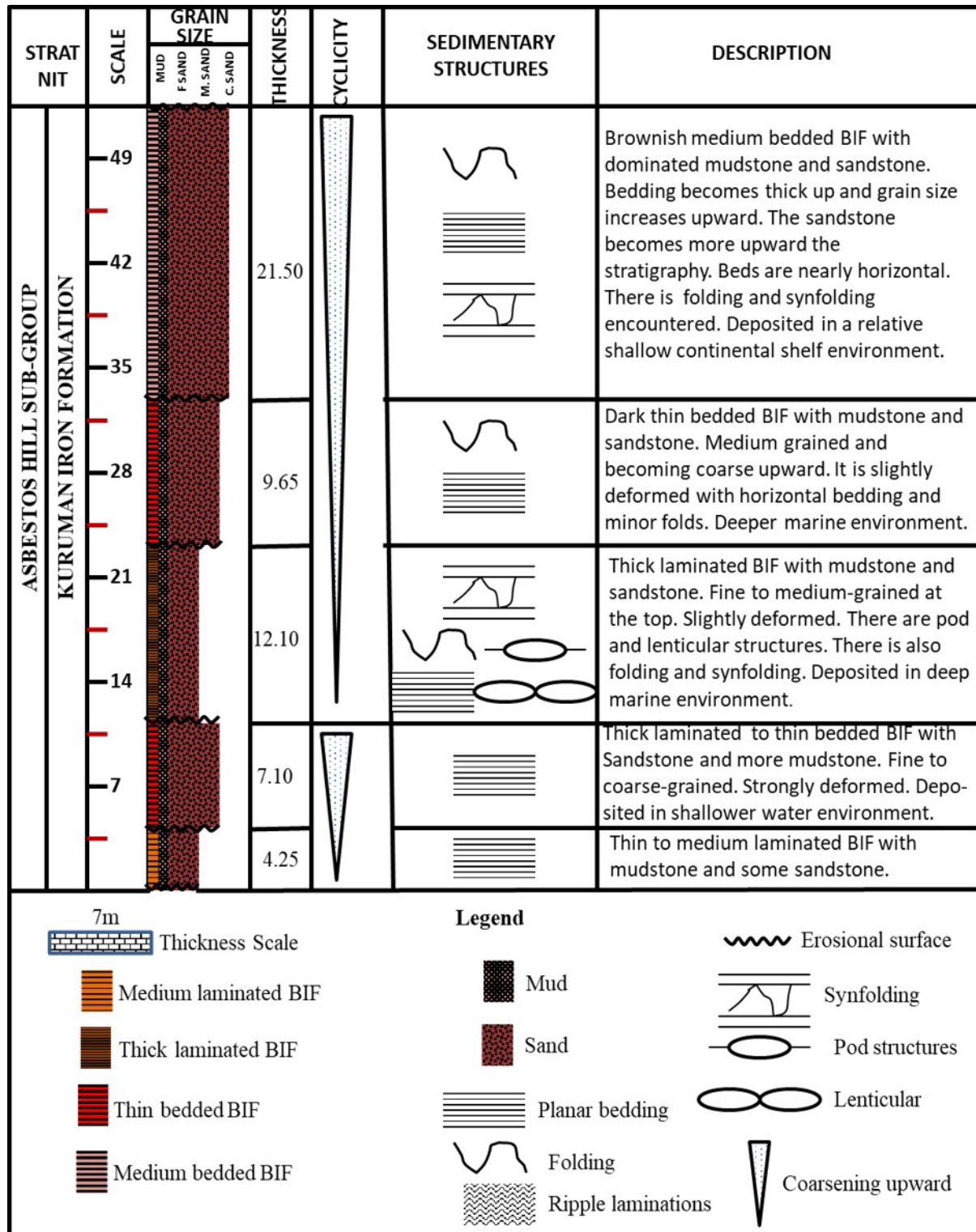


Figure 2. Measured Stratigraphic Section 1. The first measured stratigraphic section is geographically south-east of Prieska

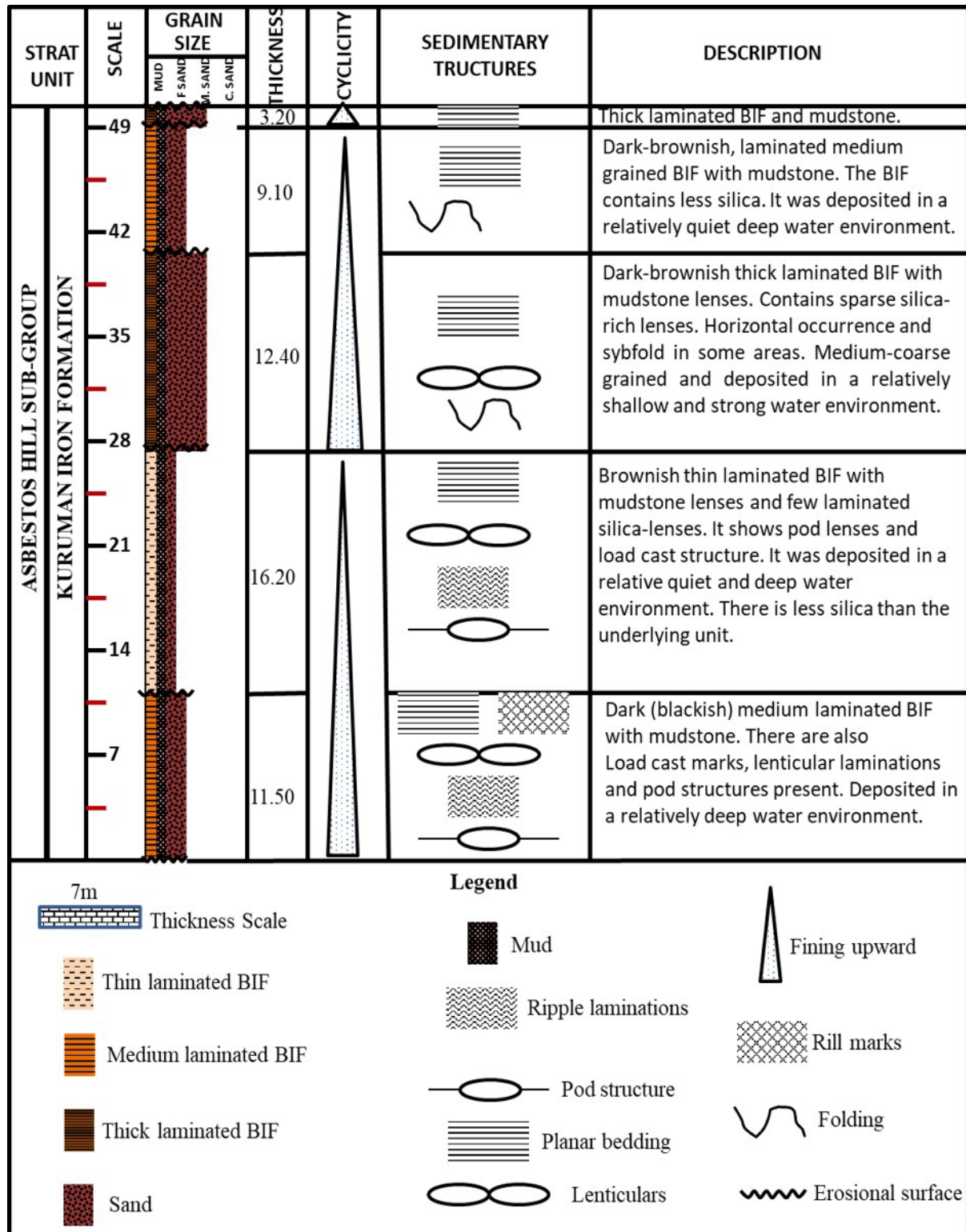


Figure 3. Measured Stratigraphic Section 2. It is geographical west of the Prieska town along Road N10

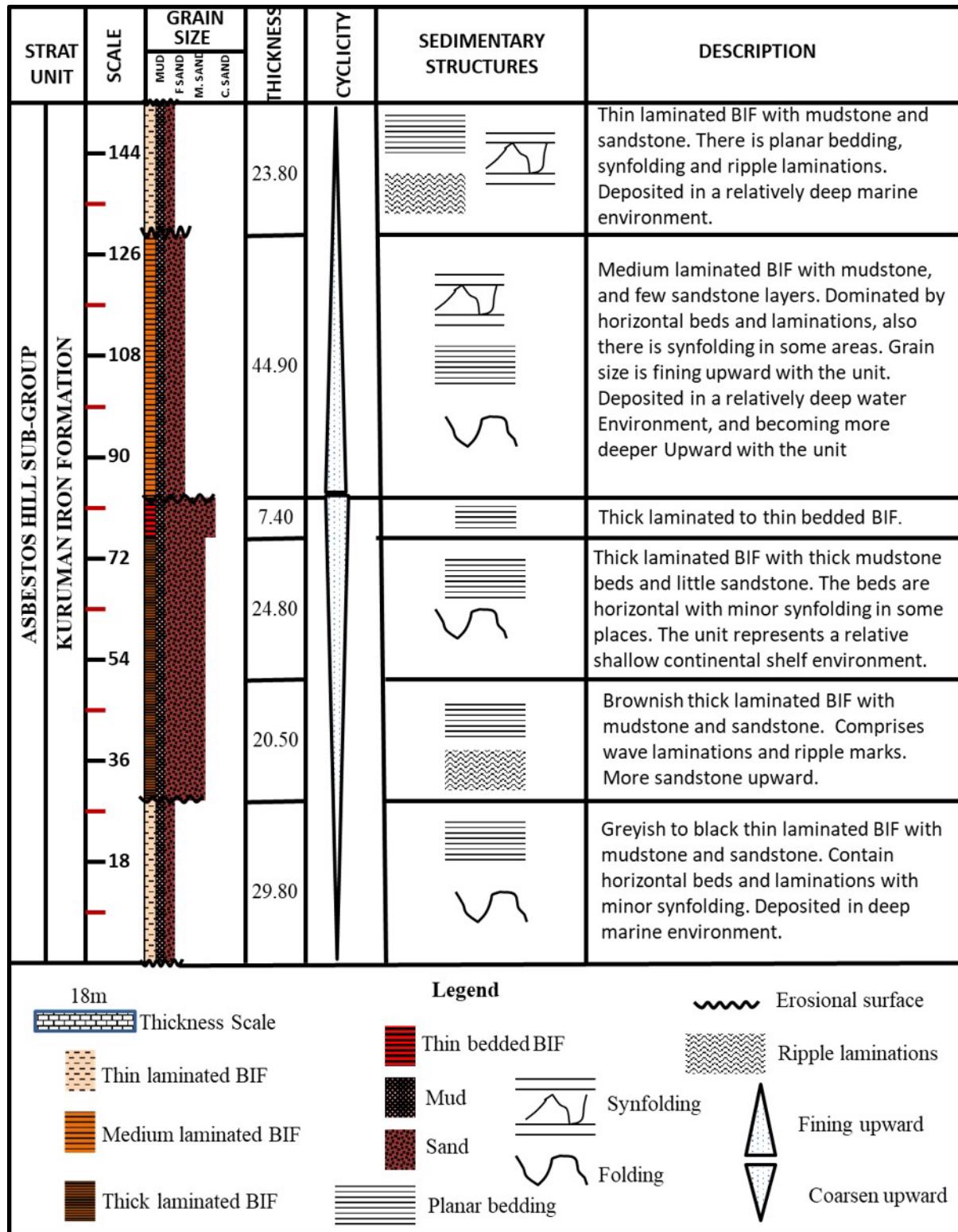


Figure 4. Measured Stratigraphic Section 3. North West of Section 2 along Road N10

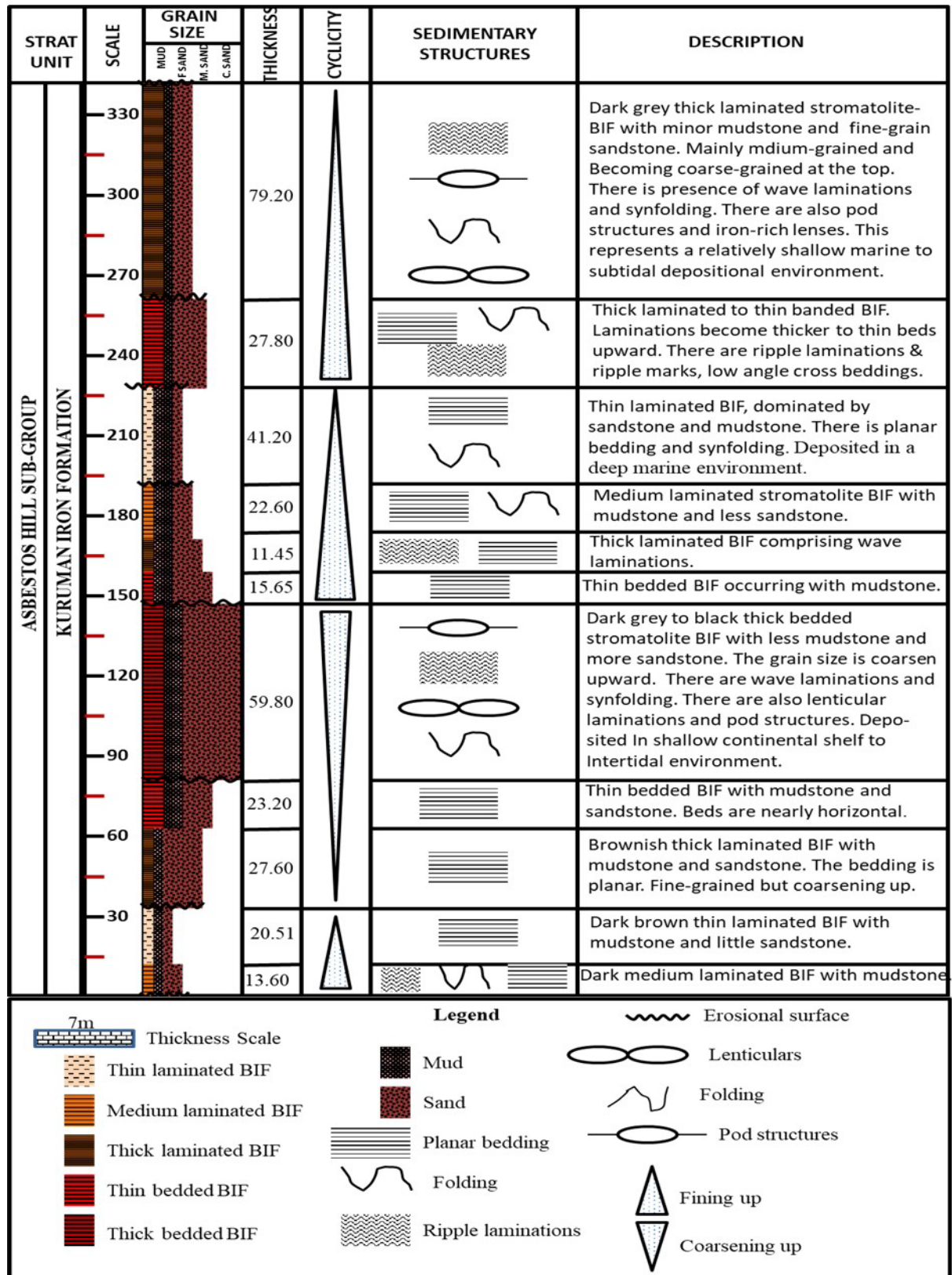


Figure 5. Measured Stratigraphic Section 4

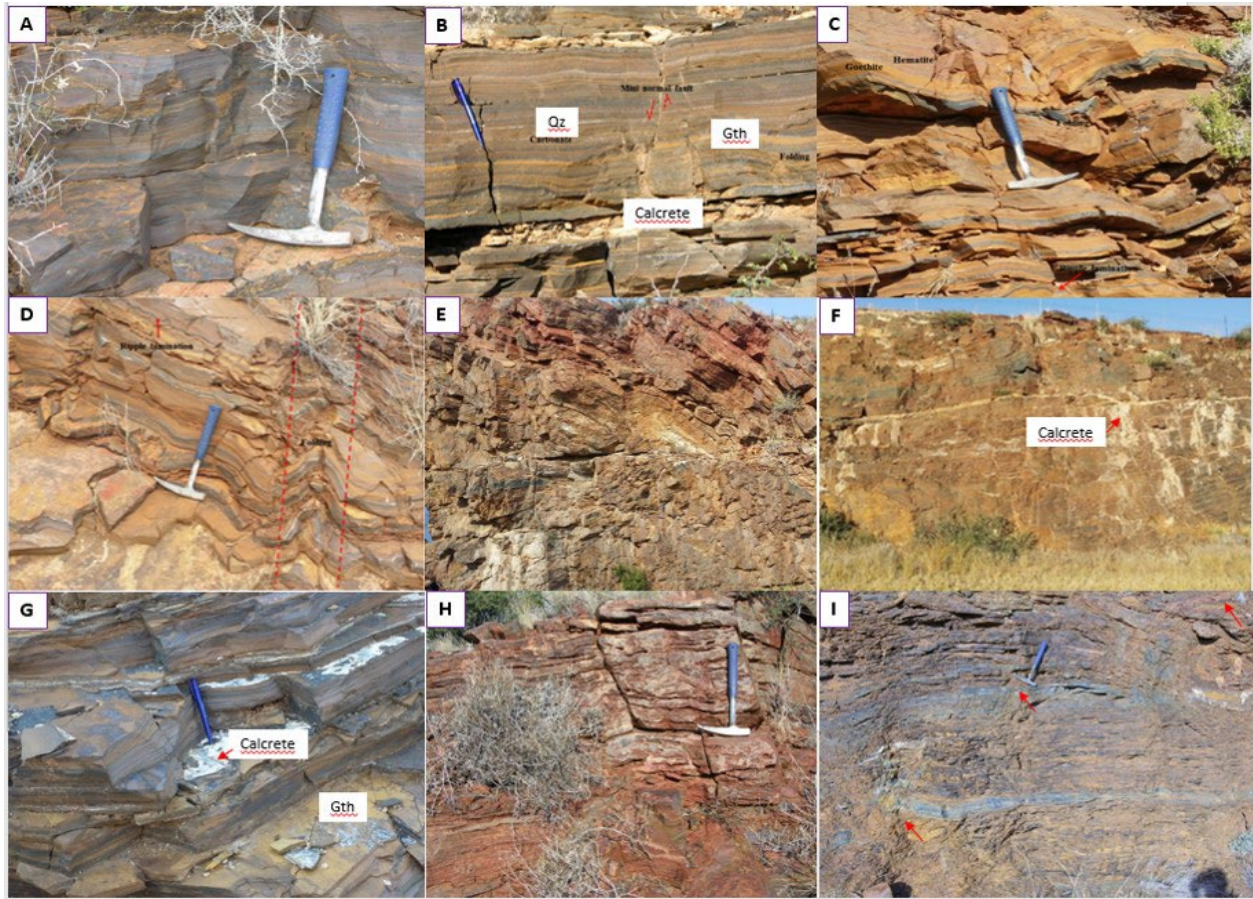


Figure 6. Field photographs illustrating (A) Horizontal laminated BIF facies; (B) Dark magnetite and reddish hematite microbands, yellow to brownish goethite-rich/limonite microbands (*Gth*), and light-coloured quartz (*Qz*) and carbonate-rich microbands. There is also calcrete between bedding planes; (C) Weathered hematite (black arrows), limonite, and goethite-rich (red arrows) formation; (D) Deformed and weathered chert, hematite, goethite, carbonate-rich mudstone with folding; (E) contact between stromatolitic banded iron formation facies, laminated dolomite stromatolite facies, mudstone, and medium to thick-bedded fine sandstone facies (F) Carbonate minerals (carb), calcrete (white area), and limonite (reddish-brown area); (G) Dark hematite, yellowish goethite-limonite and calcrete (Carb) on the bedding surface; (H) Red-brownish hematite-limonite on the weathered surface of a dolomitic BIF; (I) Blackish or grey magnetite (orange arrow), yellowish goethite/limonite (red arrow), reddish-brown hematite (yellow arrow), and chert (light brownish)

4.2. Mineralogy

The mineral assemblages of the BIF in the Kuruman Formation outcrops are mostly quartz, magnetite, goethite, and hematite, with minor traces of illite and calcite (Table 1). Quartz is a major mineral constituent amongst the samples, constituting about average 53.95wt.% (Figure 7). It appears whitish in transmitted light while being dark or greyish in reflected light and SEM photomicrographs (Figure 8). Hematite is the dominant iron oxide, displaying a reddish colouration due to weathering (Figure 9 and 10A). Hematite appears as subhedral grains and euhedral crystals due to recrystallization, whereas the anhedral forms are the common components of the hematite matrix and cement. Goethite is the second most abundant iron oxide mineral, appearing opaque in transmitted light while pale blueish in reflected light microscopy. (Figure 10D). Goethite appears as a secondary mineral, replacing the other iron oxides, silica, silicates, or carbonate minerals. It is commonly cryptocrystalline to microcrystalline, and it occurs as small, porous, subhedral to anhedral crystals or xenomorphic blasted shapes. Magnetite appears opaque under transmitted light, showing a black colour in the micro

and mesobands while pale greenish in reflected light (Figure 10C). Magnetite occurs as sub-hedral to euhedral well-formed crystals in some iron-rich bands. Magnetite commonly occurs with hematite and goethite in the strongly altered bands. Limonite is another iron oxide identified in the field and confirmed by optical microscopy and SEM-EDX. It is an impure hydrated iron mineral (with variable water content) with a colloidal, soil/powder-like, or amorphous character. Limonite is often brownish to orange-yellow in colour and earthy. It is a secondary mineral formed by the alteration of other iron oxides. Martite is a secondary hematite pseudomorph that occurs in the Prieska BIF rocks. Martite occurs in hematite-magnetite and hematite-goethite coexistences. The maghemite pseudomorph after magnetite and specularite is closely associated with martite.

Table 1. Approximate mineral abundances based on XRD results

Sample ID	Quartz wt. %	Magnetite wt. %	Goethite wt. %	Hematite wt. %	Illite wt. %	Calcite wt. %
P14	70.54	1.88	20.07	6.47	1.04	0.00
P17	49.80	15.11	22.90	12.19	0.00	0.00
P21	49.24	18.49	20.58	11.69	0.00	0.00
P25	60.09	9.64	14.88	15.39	0.00	0.00
P29	43.14	3.54	7.49	45.83	0.00	0.00
P33	41.83	12.12	18.30	27.75	0.00	0.00
P36	61.85	8.38	10.98	18.80	0.00	0.00
P42	54.20	9.08	16.34	20.37	0.00	0.00
P53	57.41	5.86	9.77	26.96	0.00	0.00
P61	51.42	29.67	11.38	3.30	0.00	4.23
Min	41.83	1.88	7.49	3.30	0.00	0.00
Max	70.54	29.67	22.90	45.83	1.04	4.23
Mean	53.95	11.38	15.27	18.88	0.10	0.42
Standard deviation	8.35	7.74	4.94	11.74	0.31	1.27

4.3. Diagenesis

The main diagenetic processes that have sturdily affected the BIF are mineral cohesion and growth, cementation and compaction, as well as the dissolution, replacement and recrystallization of minerals.

4.3.1. Mineral cohesion and growth

On the modern seafloor, iron (Fe), manganese (Mn), and phosphorite (P) bearing soft lutite/argillite have been found, particularly in the up-welling current areas [43]. The Fe (or Mn and P) elements gradually disperse/differentiate from the ferruginous lutite and move towards a nucleus. These elements go through cohesion together to become an iron-rich patch. Various patches further grow and connect, forming micro- or mesobands of the banded iron formation. The formation process of phosphorite and manganese nodules on the seafloor is similar to the BIF formation. This modern metallogenic process can be traced to the BIF in the Kuruman Formation in the Prieska area. The cryptocrystallinity and microcrystallinity features of the magnetite and hematite in the patches or microbands indicate they were primary minerals and formed in the early diagenetic stage (Figure 8A). The iron element started to disperse/differentiate from lutite (mudstone) to form magnetite or hematite patches and then connected to form magnetite and hematite microbands (Figure 8). The partially ferruginous bands are composed of the iron oxide minerals (commonly hematite and goethite) occurring with chert (quartz). These minerals are commonly occurring intermixed and display fine-grained anhedral textures (Figure 8D). The fine iron minerals in these minerals indicate that they replace the silicate minerals in the previously chert (quartz)-rich bands. The partially ferruginous bands occasionally contain a few isolated coarse-grained hematite crystals.

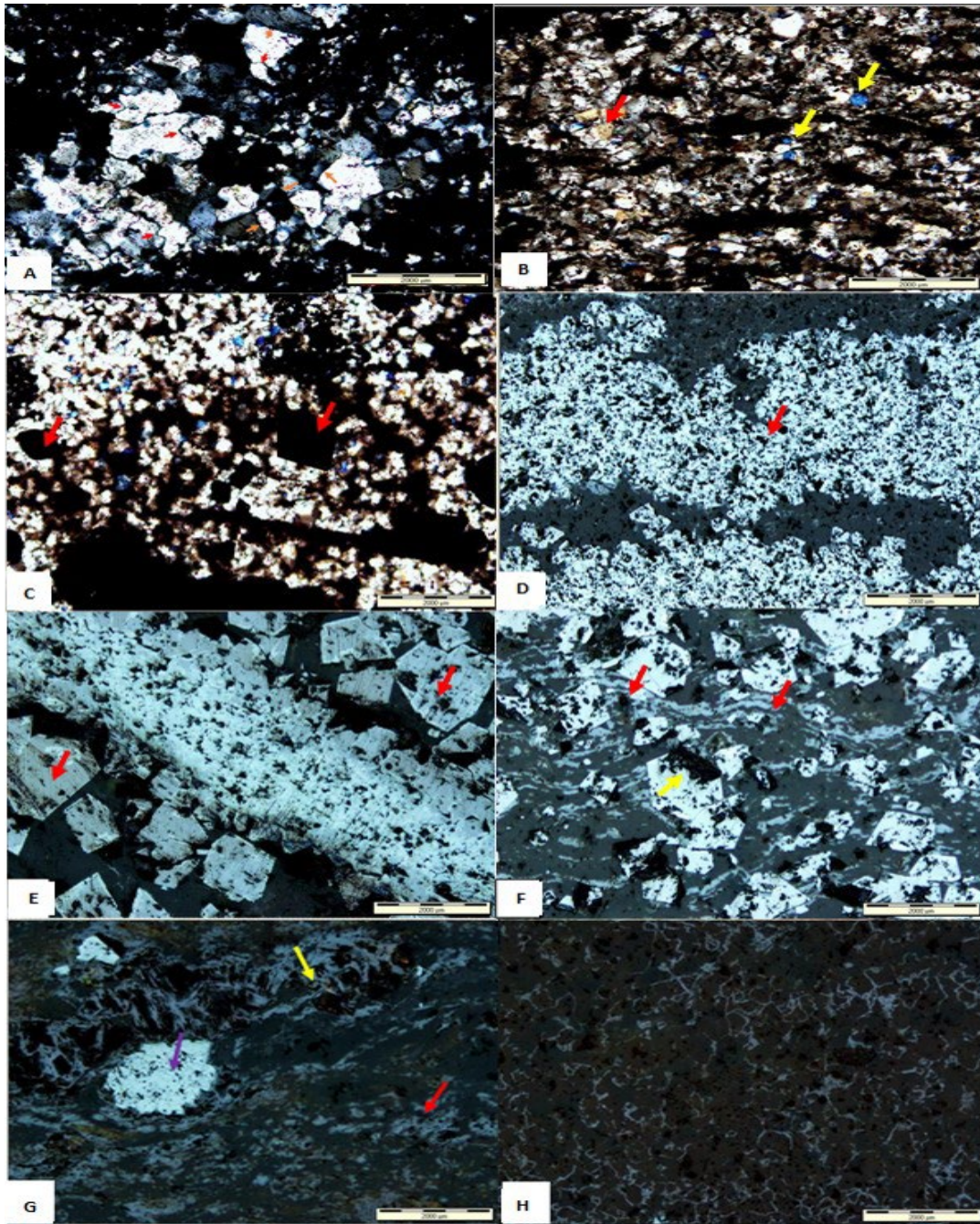


Figure 7. Thin section photomicrograph showing: (A) Long (orange arrows) and concave-convex contact patterns (red arrows) of the quartz grains in a chert-rich band; (B) Blueish riebeckite (yellow arrows), quartz, pinkish calcite (red arrow), and dark magnetite crystals; (C) rhombic hematite pseudomorphs (red arrows); (D) Porous microcrystalline hematite (red arrow); (E) Magnetite grains forming a dense martitising microband in the centre and large euhedral magnetite crystals (red arrows); (F) Goethite (red arrows) matrix and cement occurring with white subhedral to euhedral hematite (yellow arrow); (G) Leached vuggy microband with pore-filling secondary martite (purple arrow), fibrous goethite (yellow arrow) and quartz (red arrow) in the supergene zone; (H) Leached goethite-rich band

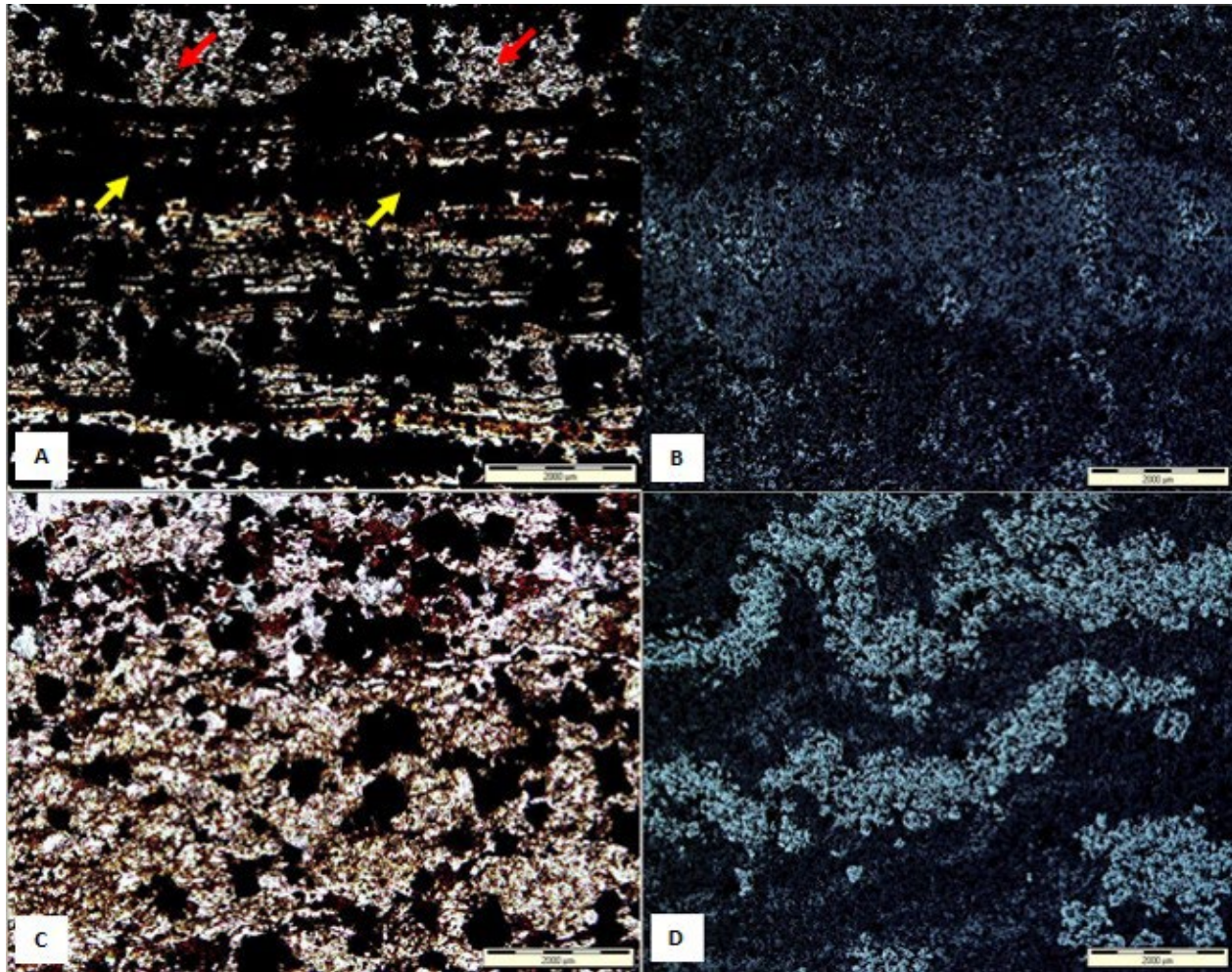


Figure 8. Photomicrograph showing (A) Dark iron oxide-rich (yellow arrows) and white chert/quartz-rich (red arrows) micro and mesobands; (B) Horizontal to wavy contacts between iron oxide-rich (whitish) and quartz-rich (dark) microbands; (C) Sediment mix of iron- oxide, chert (quartz) and mud material; (D) Cohesive hematite patches and microbands with syndepositional deformation (folding)

4.3.2. Compaction

The BIF shows variable degrees of mechanical and chemical compaction. Evidence of mechanical compaction in the samples includes the existence of different types of grain to grain contacts, the fracturing of some framework grains, as well as the deformation of ductile grains like mica. The samples display a range of grain contacts from point to sutured contacts resulting from progressive burial (Figure 9). Long contacts are common in quartz grains, signifying an intermediate burial depth. Other observed grain contacts are the concavo-convex and sutured contacts in quartz and lithic grains resulting from compaction and pressure dissolution processes in the Kuruman formation. The occurrence of sutured and concavo-convex contacts is also attributed to the deep burial diagenetic stage. Some of the quartz grains display a parallel orientation, and others comprise a chalcedonic texture. The compaction decreased the porosity and permeability within the samples. There are observed fractures on detrital quartz grains and mineral deformation is observed on the aligned quartz grains. The samples have also undergone chemical compaction, responsible for dissolution, recrystallization, and precipitation in response to overburden weight and higher stress. The compaction has also led to the carbonate minerals being dissolved and leached out of the system without replacement.

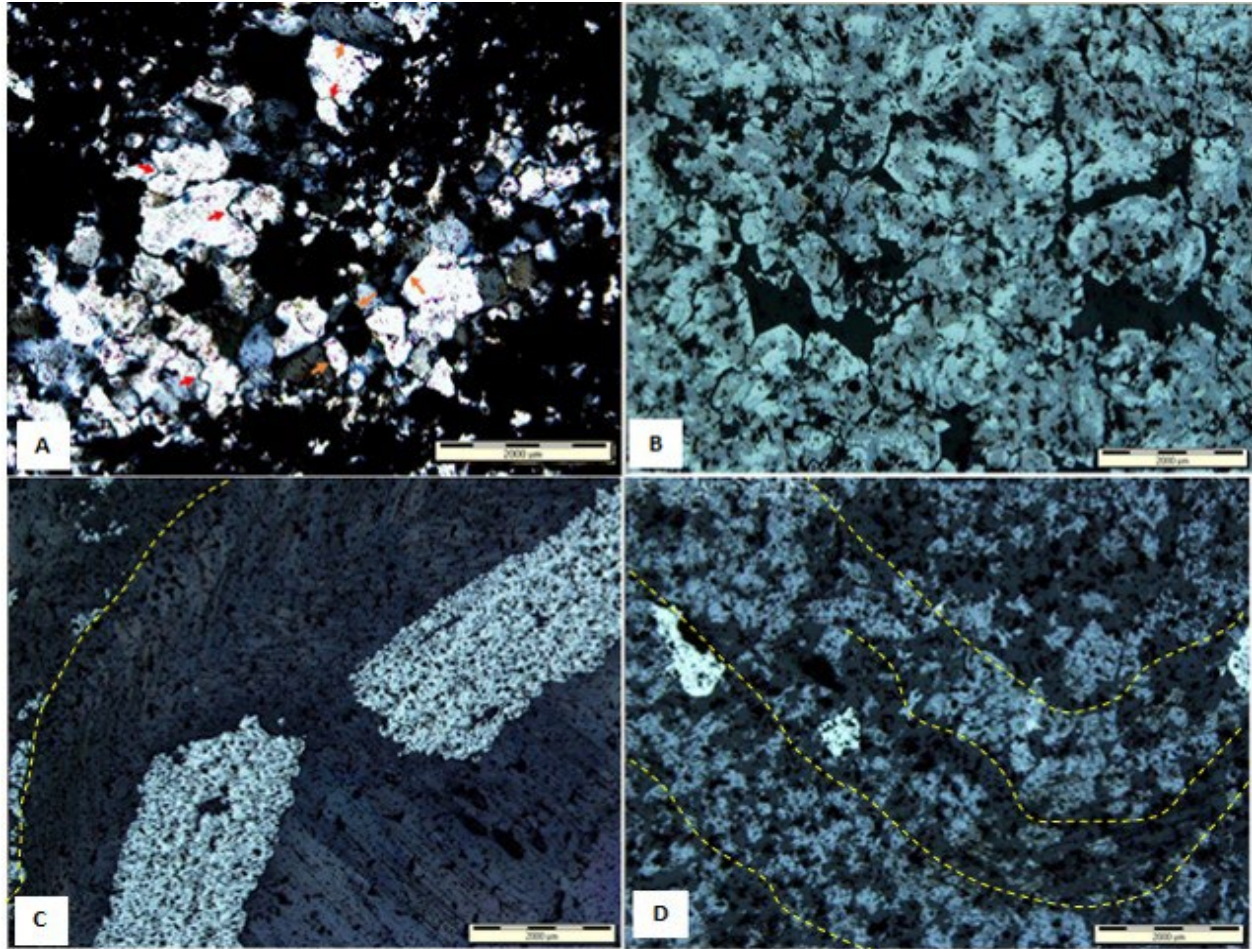


Figure 9. Photomicrograph showing (A) Long contacts (orange arrows) and concave-convex contact patterns (red arrows) of the quartz grains in a chert-rich band.; (B) Fractured grains; (C) Broken kink folds; (D) Folded goethite-rich layers.

4.3.3. Cementation and authigenic minerals

The cements that bind the framework grains of the BIF are hematite, goethite cement, cement, authigenic clay, and very rare carbonate cements. Hematite occurs as pore-filling cement or as rims around coarser quartz in a chert-rich band. It acts as a grain coating and pore-filling mineral in the pore spaces (Figure 10A). Hematite cement was developed by chemical precipitation and later by a pressure solution process during burial diagenesis. Abundant cryptocrystalline hematite is found at the centre of martite euhedral or within microcracks and small voids caused by dissolution. Some bands develop microcracks filled with crypto- or fine-crystalline hematite and dissolution holes filled with secondary flaky quartz. Goethite in the area occurs as a matrix and as cement. Goethite appears as pore-filling cement or as rims around detrital grains (Figure 10B). Goethite fills intergranular martite pore spaces or the intragranular martite pore spaces commonly at the centre of martite grains in a texture associated with coarse-bladed specular hematite. Authigenic minerals in the BIF of the Kuruman Formation are quartz, hematite, martite, and clay minerals (Figure 10C and 10D). These minerals grow from the matrix and occur as pore lining and pore-filling cement. The formation of authigenic minerals requires the necessary chemical composition and suitable diagenetic environments, such as favorable temperature and pressure of the diagenetic conditions.

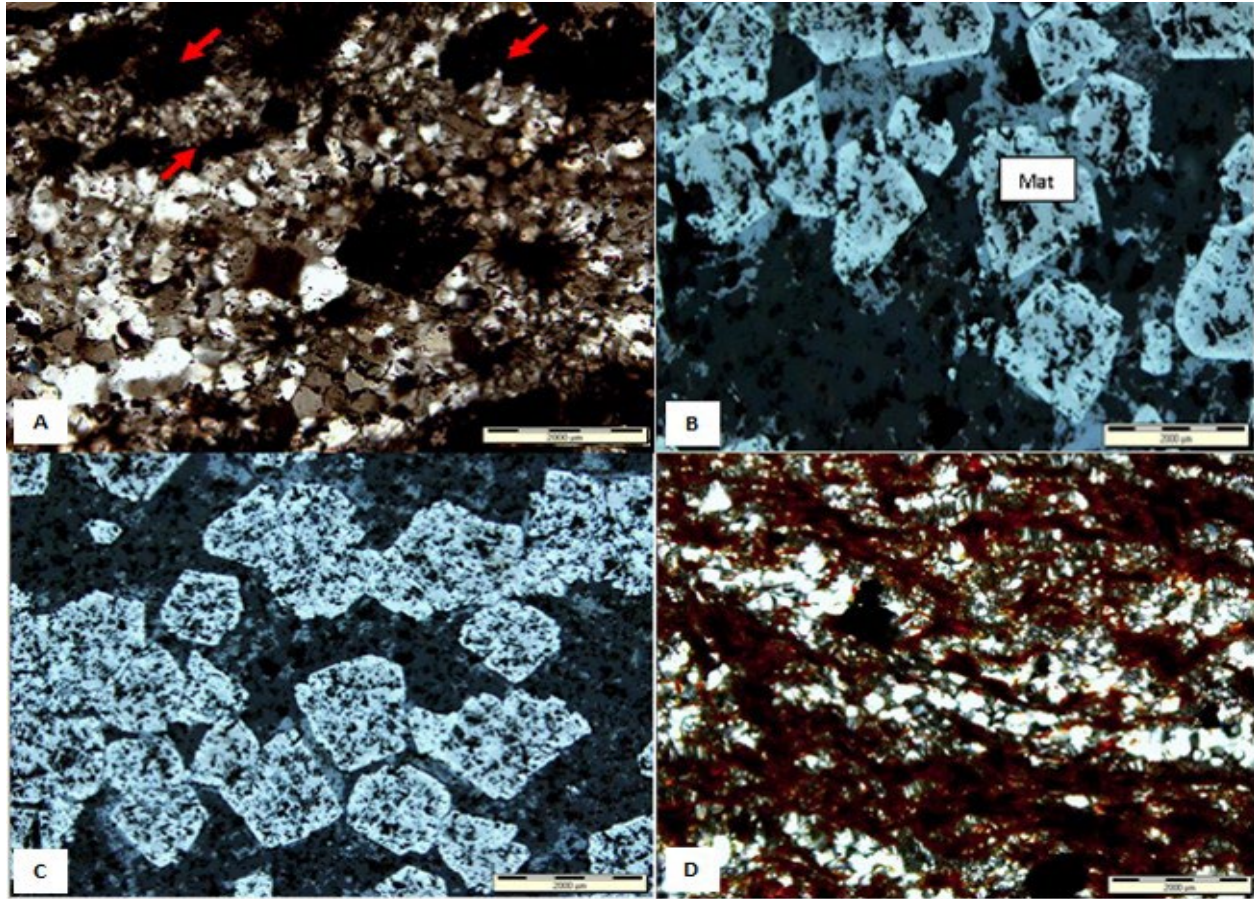


Figure 10. Photomicrograph showing (A) Hematite (red arrows) cement around the quartz grains; (B) Goethite cement occurring as pore-filling cement between martite crystals; (C) Authigenic martite with subhedral to euhedral crystalline shapes; (D) Hematite and quartz

4.3.4. Dissolution

Dissolution is a common diagenetic process in the studied samples, and it encompasses the removal in solution of part or all of the previously existing minerals, creating secondary pores in the rocks (Figure 11). The main soluble components in the samples are carbonate, and iron silicate minerals. SEM observation revealed that carbonate and iron silicate minerals are dissolved and destroyed during dissolution, creating cracks or cavities and pore spaces between the mineral grains. The pore spaces are generally grouped into primary pores and secondary pores based on their formation. The occurrence of the pore spaces and pore networks in the Prieska BIF would mostly be influenced by the dissolution of the carbonate and silicate minerals during diagenesis. They are also impacted when iron oxides and quartz replace the susceptible carbonate and silicate minerals. Pore spaces can be between the grains (inter-pore spaces) and within the crystals (intra-pore spaces). These pore spaces can be later filled by one of the BIF minerals, particularly iron oxides or silica.

4.3.5. Mineral replacement

The in situ dissolution of one mineral and the rapid precipitation of the other is known as mineral replacement. The dissolution could occur over time, with new minerals precipitating and progressively replacing the existing or dissolving minerals. In these samples, the replacement of one mineral by another is a rather frequent diagenetic phenomenon. As burial depth increases, so does the ambient temperature, causing some existing minerals to deteriorate and become unstable. In the new diagenetic environment, these unstable minerals are gradually displaced and replaced by more stable minerals. Mineral replacement might be partial or

comprehensive, depending on the situation. While partial replacement preserves the identification of the original minerals, complete replacement eliminates the identity of the original minerals, resulting in a distorted image of the rock's original mineralogy. Petrographic and SEM analyses have revealed the replacement of other minerals by hematite, goethite, magnetite, and silica (quartz).

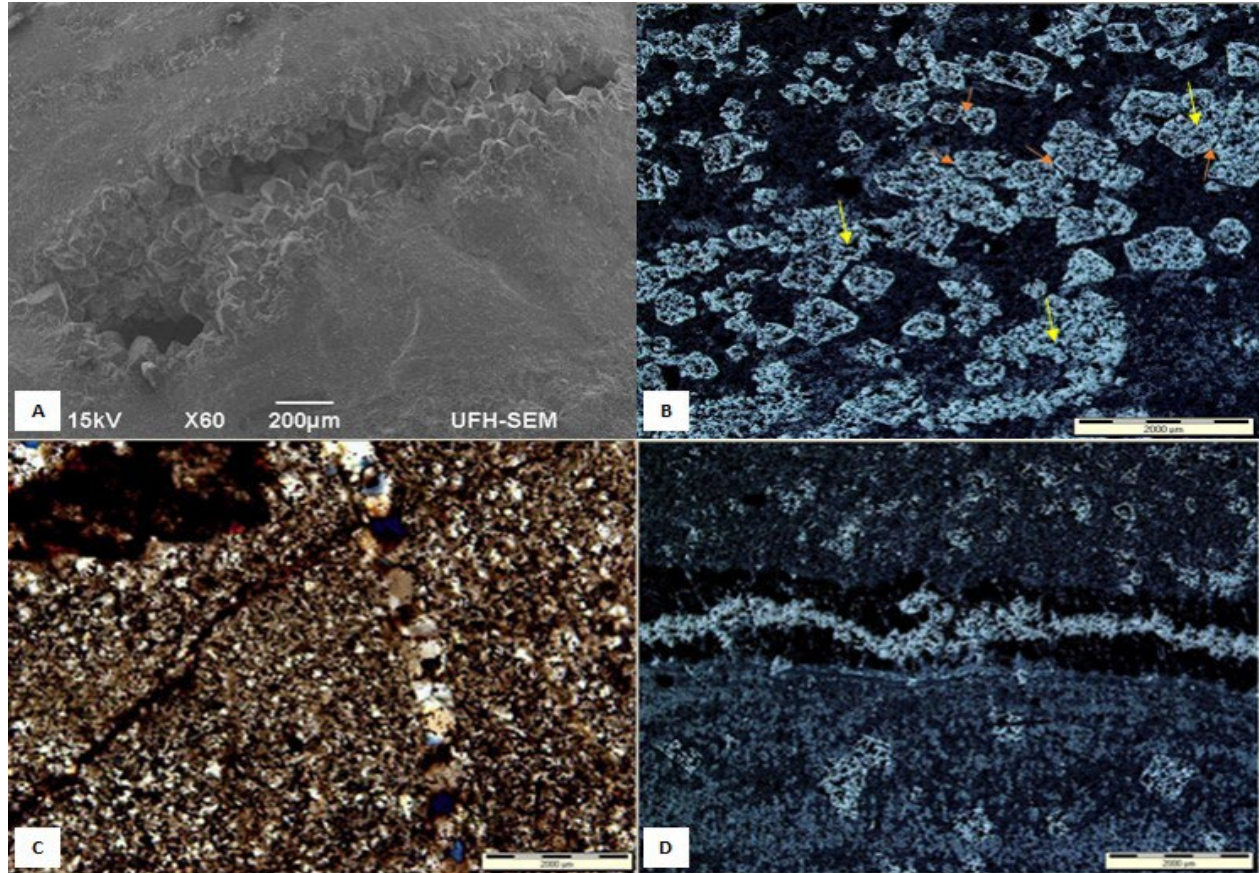


Figure 11. Photomicrograph showing: (A) Dissolution hole filled with quartz; (B) Inter-pore spaces (red arrows) and intra-pore spaces in the hematite-rich (yellow arrows) mesoband; (C) Microcrack filled with fine hematite; (D) Horizontal microcrack filled by fine hematite and dissolution holes filled by quartz.

4.3.5.1. Replacement by hematite

Thin section observation revealed that secondary hematite is formed by replacing the coarser magnetite, while it is also formed through maghemite depending on crystallite size. The original magnetite changes to martite and into laths of specularite or in part to lacunar phases between magnetite and maghemite (kenomagnetite/maghemite), which commonly alters to goethite at a later stage (Figure 12A). In these changes, magnetite occurs as relics at the centre of martite crystals. The replacement commences from the periphery inwards and passes through the martite stage to the hematite's final product. The commonly coarser-grained magnetite than the coexisting chert and hematite reflects a possible crystallization at the later diagenetic stages of hematite. The break-up of martite crystals after martitization might have distorted the crystal structure. Hematite also occurs as the secondary replacement mineral for the carbonate minerals and silicates and is part of quartz [10]. The carbonate mineral replacement by hematite is reflected by the different sized rhomb-shaped hematite grains (Figure 12B-C). The replacement of the silicate minerals by hematite within the quartz-rich bands resulted in the hematization of those bands. Also, the fine-grained hematite present in some of the martite- hematite-goethite bands is a product of goethite conversion.

4.3.5.2. Replacement by goethite

Goethite occurs as the secondary mineral replacement for magnetite and hematite/martite. In a zoning transformation, magnetite was transformed by hydration into goethite and subsequently into martite by dehydration. Goethite replaces maghemite in the martitising areas. The carbonates and silicate minerals are susceptible to mineralogical and textural changes. Hence, they were later volumetrically replaced by the iron oxides, including goethite, with minor textural changes (Figure 12D-E). Like hematite replacement, goethite replacement for the carbonate assemblage is indicated by the rhomb-shaped goethite crystals. The hematitized original quartz-rich bands also reflect the replacement of the silicates by hematite.

4.3.5.3. Replacement by quartz

Quartz occurs in the Prieska BIF as a replacement mineral in some of the bands. It commonly replaces the susceptible carbonate and silicate minerals (Figure 12F). The rhombic-shaped silica-rich area reflects a typical replacement of the carbonate minerals by quartz. The iron oxides are also rarely replaced by silica during favourable conditions of diagenesis.

4.3.6. Recrystallization

Mineral recrystallization is observed in the samples, and it is defined as a change in the size or shape of crystals of a given mineral without a significant change in their chemical composition. Some minerals are dissolved and rearrange their crystal lattice as a result of changes in temperature, pressure, and fluid phase composition, resulting in a series of interlocking crystals that are often larger than the original grains. These existing minerals can keep their chemical composition while changing in size only. Some existing minerals, on the other hand, can be completely changed or transformed into new minerals with a different chemical composition. Recrystallization was indicated by the transformation of cryptocrystalline hematite to micro-crystalline and fine crystalline hematite into coarse crystalline hematite under increased temperature and pressure. Notably, within the samples is the recrystallization of cryptocrystalline quartz to form micro- or fine-crystalline, coarse-grained quartz, and chalcedony quartz (Figure 13). Quartz shows well-crystallized and coarser grains, which signify recrystallization during late diagenesis (Figure 13A). The coarse-grained quartz also occurs in quartz veinlets, representing the late diagenetic features or post-depositional alteration (Figure 13B). Iron oxides experienced recrystallization to accommodate changing structural and diagenetic conditions. They formed from each other during different diagenetic conditions and went through grain merging by growth and oxidation to kenomagnetite/martite or (oxy-) hydration to goethite (Figure 12A). With the increase in burial depth, hematite could have gradually recrystallized from the goethite-rich matrix (Figure 12D). Another common recrystallization phenomenon in the Prieska BIF is siderite transformation with increased burial temperatures to form coarse-grained ankerite.

4.4. Mineral paragenesis

The mineral paragenesis represents a genetic sequence or pathway of the mineral assemblages formed over geological time. The mineral paragenesis is deduced from the deposition and diagenetic events and arranged based on the formation time. Thus, the paragenesis sequence (Figure 114) shows the primary and post-depositional minerals of the Prieska BIF and their relative formation times as well as the relationship among the different assemblages. The mineral assemblages in the BIF can be grouped into primary, diagenetic, low-grade metamorphic mineral assemblages, and weathering mineral assemblages (Figure 14).

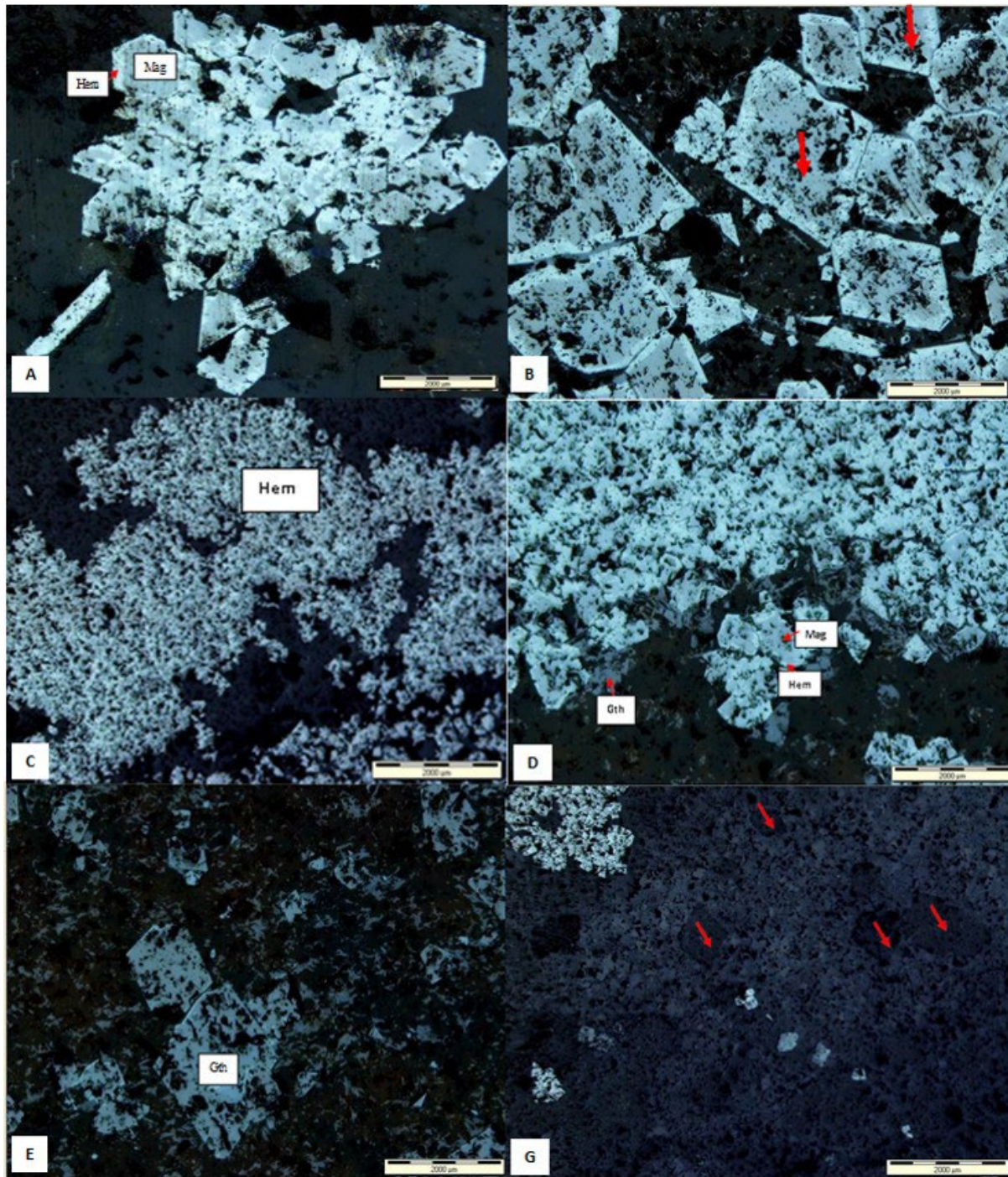


Figure 12. Thin section photomicrograph showing: (A); Inner magnetite/kenomagnetite and outer hematite in the martitising bands. (B) Rhombic iron-oxide (hematite) pseudomorphs (red arrows) after replacing carbonate mineral precursor; (C) Porous microcrystalline earlier magnetite replaced by fine hematite; (D) Goethite replacing magnetite/kenomagnetite in the martitising bands; (E) Rhombic-shaped carbonate minerals replaced by goethite; (F) Rhombic-shaped carbonate minerals replaced by quartz.

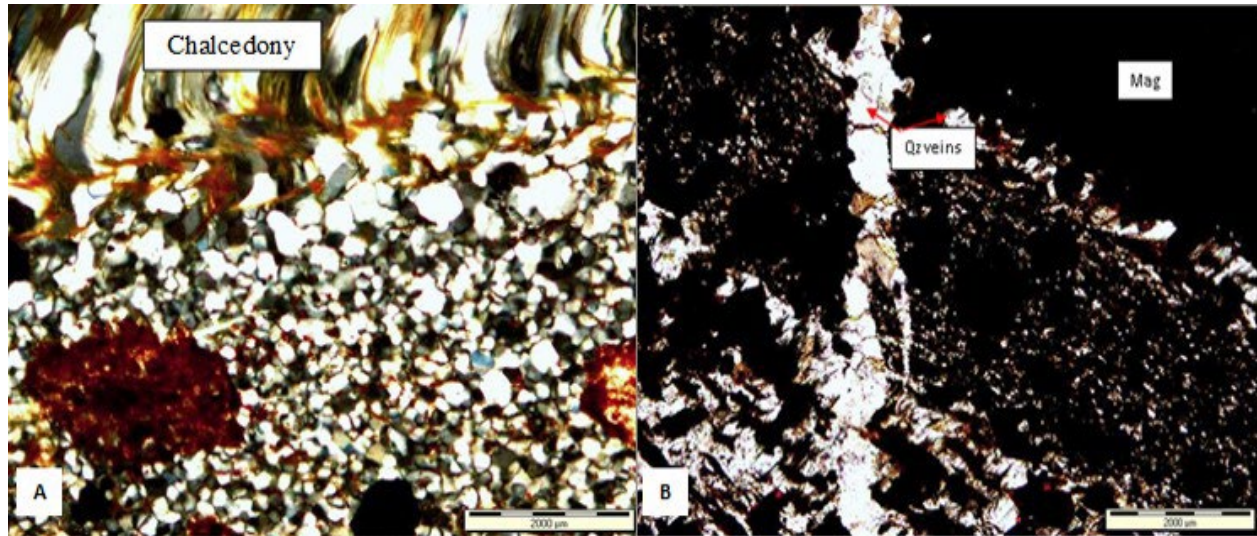


Figure 13. Thin section photomicrograph showing: (A); different quartz sizes and shapes and fibrous chalcedony; (B) Horizontal and vertical quartz veinlets related to recrystallization during diagenesis

4.4.1. Primary mineral assemblage

The mineral assemblages of the rocks are composed of various primary and secondary minerals. These primary minerals include hematite, magnetite, chert (amorphous quartz), calcite, siderite, and smectite. From the petrographic evidence, hematite and magnetite are interpreted as the primary minerals. Also, the cryptocrystalline to microcrystalline chert (quartz) indicates primary precipitation. The optical zonation displayed by siderite from the petrographic study is evidence for siderite formation as a primary precipitate. This zonation reflects the immediate changes in the seawater or pore fluid chemistry [17]. It indicates that siderite is one of the earliest mineral precipitates of the Prieska BIF sediment. Petrographic examination revealed no evidence for a carbonate precursor or significant grain replacement by the siderite. The siderite appears to have formed entirely through direct precipitation in the bottom water or intergranular pore water. The siderite zonation shown by the petrographic examination reflects the possibility of two principal siderite types (Fe-rich and Mg-rich). Invariably, paragenetic relationships in samples containing both types indicate that the Fe-rich siderites formed before the Mg-rich variety. Stilpnomelane was formed as a primary silicate precipitate based on textural grounds and in the absence of a possible precursor. Stilpnomelane is stable at 25°C from low to high Eh at alkaline pH in the iron-formation system.

4.4.2. Diagenetic mineral assemblage

The diagenetic mineral assemblage includes all those minerals formed from the primary or pre-existing minerals during diagenesis. These minerals are hematite cement, magnetite, quartz cement, ankerite, recrystallized clay mineral, illite, riebeckite, and stilpnomelane. Chert, a primary silica mineral, recrystallized into quartz, and its crystalline size gradually changed from fine-grained to coarse-grained as diagenesis progressed from early to late. The quartz veins are also associated with late diagenesis and metamorphism [3, 12]. The ferrihydrite precipitates into goethite and small hematite at pH 4, while major hematite crystallizes at pH 7–8. Therefore, hematite is interpreted as a secondary mineral formed under near-neutral pH conditions after initial precipitation. Magnetite could be formed from hematite or ferrous carbonates such as siderite. Magnetite formation could be driven by partial reduction of hematite by organic carbon. It could also be formed through the partial oxidation of Fe (II) or Fe (III) minerals by CO₂. It could be produced by siderite oxidation at 450 °C and 2 kbar [21].

The flaky or fibrous chalcedony was recrystallized from chert, and it will further crystallize into quartz. Chalcedony lines up parallel to deformation and local tectonic pressure (Figure 10B). These are interpreted as diagenesis or post-depositional recrystallized quartz varieties.

Some authigenic siderite growth occurred during early diagenesis and burial. The impure, Mg-enriched nature of the siderites is typical for early diagenetic siderites from marine depositional environments. Diagenetic maturation thus results in an increasing crystallinity of siderites. No sign or evidence reflects chert substitution by siderite within the Prieska BIF. The coarser-grained ankerite represents the late diagenetic minerals. Petrographic observation shows that ankerite formed during the deep burial and compaction of the samples, forming larger grains and distorting the primary microlamination. The ankerite could represent a by-product of siderite dissolution and subsequent CO₂ release. The secondary calcite variety was formed during early to late diagenesis. Minnesotaitite represents the late stages of diagenesis, possibly being formed from stilpnomelane or primary greenalite at 200°C to 230°C temperatures [47]. Minnesotaitite and possibly riebeckite developed through the late stages of diagenesis or low-grade metamorphism that resulted from the rocks' deep burial. On the basis of mineral assemblages and textural relationships, Riebeckite formed during late diagenesis or very low-grade metamorphism (around 150 °C) [11]. [11] reported that riebeckite was probably formed when iron-oxides reacted with silica and water. It could have formed through (1) the reaction of carbonates (siderite), silica, and water, (2) the reaction of iron-oxides, carbonates, silica, and water, (3) through the reaction of iron silicates (stilpnomelane), carbonates, and silica, and (3) through the reaction of iron-oxides and stilpnomelane [11].

The first three reactions are the most likely for the formation of riebeckite in the area. Hematite and magnetite are the sources of iron, while quartz is the source of silica. The carbonates could be an important source of magnesium and iron for riebeckite. In general, riebeckite related to carbonates has a higher MgO content than that of carbonate-free associations. Siderite may be an important reactant among the carbonates during diagenesis because of its common existence. The common constituents of most riebeckite assemblages are ankerite and calcite. The massive riebeckite bands result from riebeckite replacing the primary minerals in quartz-iron-oxide mesobands. Riebeckite uses magnetite and other minerals as nucleation and growth sites. Riebeckite was affected by weathering and replaced by iron oxides or leached out when exposed to the earth's surface. Illite is formed from smectite through cation substitution, releasing Mg²⁺ and Fe²⁺ into solution at major depth during late diagenesis [48-49].

4.4.3. Low-grade metamorphic assemblage

The low-grade metamorphic mineral assemblage within the Prieska area includes riebeckite and minnesotaitite. The flaky and fibrous chalcedony quartz, on the other hand, has been interpreted as the later tectonic overprinting or deformation quartz. Quartz is affected by burial stress conditions such as pH, temperature, and pressure [50]. The flaky, fibrous quartz and long quartz fringes are more pronounced parallel to deformation and pressure shadows adjacent to the iron oxide micro-bands (Figure 10B). These are late secondary diagenesis or post-depositional recrystallized quartz varieties. Minnesotaitite and riebeckite may have formed as a result of late diagenesis or low-grade metamorphism caused by the rocks' deep burial. Minnesotaitite developed during later low-grade metamorphism that resulted from the rocks' deep burial. It must have formed from primary greenalite and iron-rich chlorite during late diagenesis to early metamorphism at 200°C to 230°C temperatures [50]. Riebeckite was formed during late diagenesis or very low-grade metamorphism on mineral assemblages and textural relationships [43]. The riebeckite formation may also be related to deformation, as evidenced by the petrographic examinations [11].

PARAGENIC ASSEMBLAGE					
MINERAL PHASES	MINERAL TYPE	PRIMARY MINERAL ASSEMBLAGE	DIAGENETIC MINERAL ASSEMBLAGE	LOW-GRADE MINERAL ASSEMBLAGE	WEATHERING MINERAL ASSEMBLAGE
Iron oxides	Hematite				
	Martite				
	Magnetite				
	Goethite				
	Limonite				
Silica	Quartz				
Carbonates	Siderite				
	Ankerite				
	Calcite				
Silicates	Calcrete				
	Stilpnomelane				
	Riebeckite				
	Smectite				
	Illite				
	Minnesotaite				

Figure 14. Mineral paragenetic assemblages of the Kuruman BIF the in Prieska area. The line thicknesses and lengths correspond to the relative abundances of the indicated minerals

4.4.4. Weathering mineral assemblage

The weathering mineral assemblage involves all the minerals formed due to uplift, weathering, and oxidation [51]. These minerals include hematite, goethite, limonite, martite, and calcrete. The quartz shows no evidence of major alteration by weathering. Silica is rarely removed and replaced by fine-grained iron oxides. A rare alteration process in the area is the apparent volume-for-volume replacement of chert by iron minerals. Hematite could be formed directly from magnetite through oxidation. At the same time, it could also be formed by maghemite replacing parts of magnetite grains, leaving islands of unreplaced magnetite (kenomagnetite) depending on crystallite size [52-53]. Hematization of chert banding resulted from hematite replacing silicate minerals within cherty bands. Due to heat, the red hematite also forms from the yellow dehydrated goethite. Hematite replaces the carbonate minerals as well. Goethite forms from the ferrihydrite at pH 4. A fine-grained groundmass is formed by widespread goethite that replaced hematite and remnant magnetite during weathering. Goethite was probably formed at low temperatures by hydration of the partly oxidized magnetite, martite, maghemite, and hematite phases. Some carbonates were volumetrically replaced by goethite with minor textural changes. Some of the iron silicates were also replaced by goethite.

Magnetite was formed by converting hematite through hematite and siderite reaction [52]. Magnetite overgrowths along the boundaries of hematite- and chert-rich laminae are evidence of this conversion. This reaction (FeCO_3 ; siderite) + Fe_2O_3 ; hematite) = Fe_3O_4 ; magnetite) + CO_2 is favoured at relatively high temperatures and pressures [51]. In the supergene and weathering environments, magnetite oxidizes to martite and, in part, to goethite. Magnetite appears to diminish as supergene alteration and weathering intensifies, and it is replaced by hematite and goethite. Quartz is hardly affected by weathering, and it shows no evidence of dissolution or being replaced by another mineral. Siderite is chemically unstable in air and rapidly oxidizes to the secondary magnetite, maghemite, hematite, and goethite either before, during, or after uplift. Siderite is rapidly destroyed by oxidation. It can be inferred that most post-diagenetic oxidizing effects, such as weathering during uplift and exposure of a sedimentary sequence, destroy the mineral. The ankerite is depleted relative to siderite at low temperatures (at 25°C) [54-55]. Like siderite, ankerite is replaced by iron oxides during supergene processes, weathering, or leaching without replacement. The secondary calcite was later replaced by the iron oxide minerals or leached out of the system. This leaching and replacement were due to uplift or weathering. These rhomb-shaped minerals occur in different sizes, indicating different stages of formation. The iron silicates have been traced to the early stages of BIF formation. These were later compacted and replaced by the iron-oxides and quartz, or leached out of the system.

4.5. Origin and formation process of the BIF

Multiple formation processes were involved in the banded iron formation's origin within the Prieska area. The first process involves the deposition of iron-rich and silica (chert/quartz)-rich mud materials on the deep ocean floor. This deposition was accompanied by the formation of a mixture of iron-rich mud (felutite) on the seafloor (Figure 15A) [56-57]. The second process involves differentiation of the felutite and the formation of disseminated iron-oxide from mud (Figure 15B). The third process includes cohesion and diagenesis of disseminated iron-oxide and the formation of iron-rich (magnetite/hematite) and silica-rich (chert/quartz) patches, lenses (pod structures), microbands, and laminations (Figure 15C and D). The fourth process is consolidation and compaction, leading to the final banded iron formation (BIF) (Figure 15E and F).

According to petrographic evidence, felutites contained a mixture of iron oxide minerals, silica, carbonate, and silicate minerals. This felutite mixture experienced progressive differentiation, cohesion, and diagenesis. Then the iron-oxides and chert (quartz) gradually separated from the mud (felutite). The quartz association with iron oxide assemblages indicates that these minerals were deposited mixed and underwent differentiation due to favourable precipitation conditions. This association also suggests that they were replacing each other in different conditions. The BIF micro and mesobands' arrangement into discrete bands, diffusive bands, patches, lenticular and pod-shaped bands, and laminations indicate the BIF development in different diagenetic stages. The realignment of the chert (quartz), silicate, and iron-oxides resulted from diagenesis or compaction. The Prieska BIF is constituted of primary and secondary minerals such as hematite, magnetite, martite, goethite, limonite, quartz, stilpnomelane, riebeckite, minnesotaite, illite, siderite, ankerite, and calcite. The secondary origin of the minerals is a result of neomorphism, recrystallization, and replacement. The dominant quartz and iron oxide concentrations displayed by petrographic studies and geochemical data are attributed to their primary precipitation and replacement of the carbonates (siderite, ankerite, and calcite) and silicates (riebeckite, stilpnomelane, and illite) by those minerals during diagenesis and metamorphism.

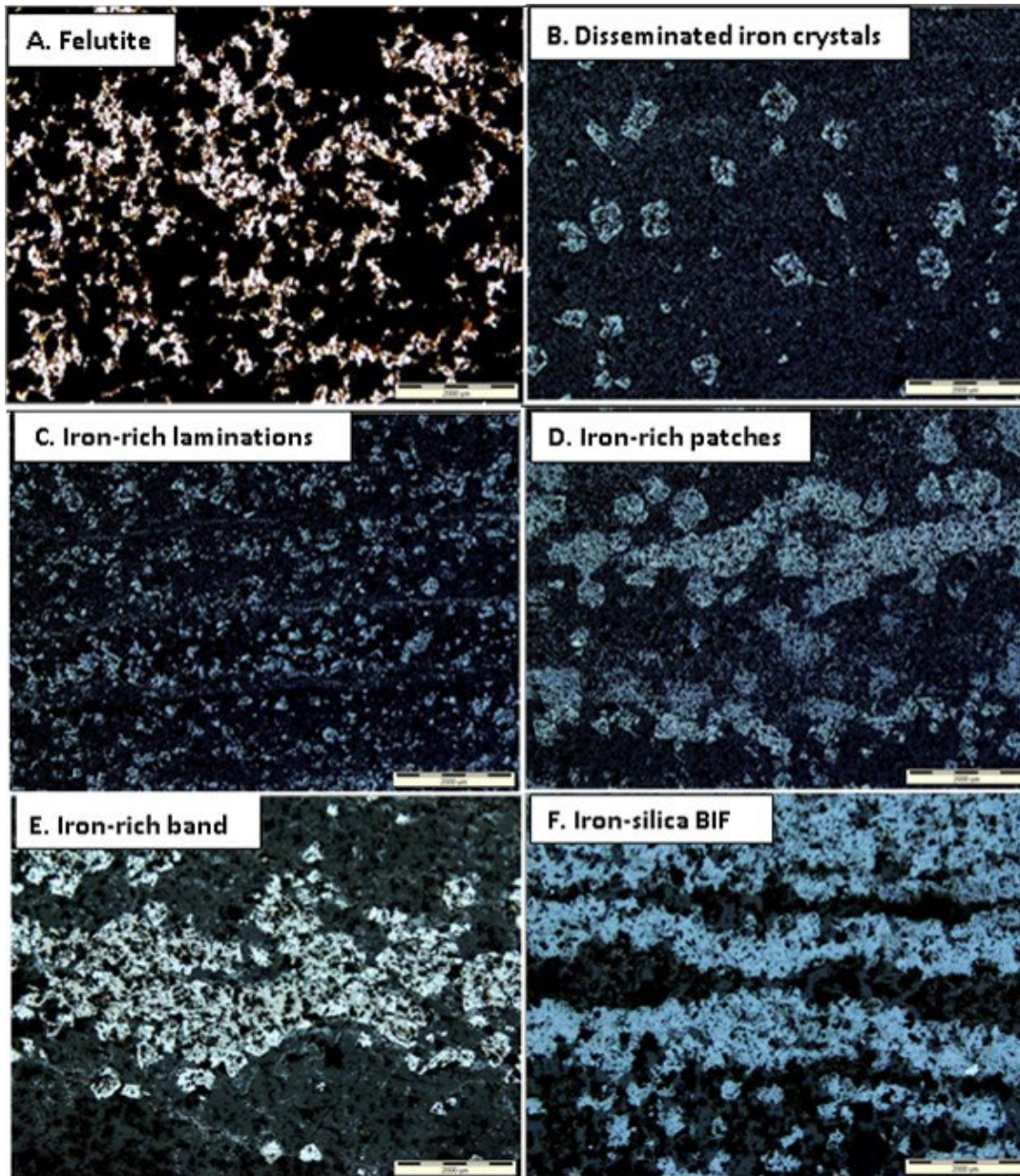


Figure 15. Origin and formation processes of Banded Iron Formation: (A) Iron-rich mudstone (felutite) showing the mixture of iron oxides, chert (quartz) and silicate minerals; (B) Authigenic hematite grows up as disseminated crystals from felutite through recrystallization; (C) Hematite crystals cumulated together to form laminations; (D) Hematite clusters together to form iron-rich patches and lenses; (E) Hematite/goethite further grows to become various sized bands; (F) Iron-rich mesobands alternating with silica bands and finally the formation of banded iron formation

5. Conclusions

Petrographic and diagenetic studies revealed four groups of mineral paragenesis. These groups include primary mineral assemblages (i.e., magnetite, hematite, siderite, chert/quartz, stilpnomelane, and smectite), diagenetic mineral assemblages (i.e., martite, quartz, illite, calcite, and ankerite), low-grade metamorphic mineral assemblages (i.e., riebeckite and minnesotaite), and weathering/supergene mineral assemblages (i.e., goethite, limonite, calcite (calcrete), quartz (silcrete), and clay minerals). Post-depositional and geochemical studies indicate three processes responsible for the mineralogy and geochemical changes of the Prie-

ska BIF. These processes include diagenesis, low-grade metamorphism, and surficial weathering and oxidation. These studies also show that most of the mineral assemblages are of secondary origin. Multiple formation processes were involved in the origin of the banded iron formation: (1) deposition of iron-rich mud material in the deep ocean floor and formation of a mixture of iron-rich mud (faluite) on the seafloor; (2) differentiation of faluite and formation of disseminated iron-oxide and chert (quartz) from mud; (3) cohesion and diagenesis of disseminated iron-oxide and formation of iron-rich (magnetite/hematite) and silica-rich (chert/quartz) patches, lenses (pod structures), microband, and laminations; (4) consolidation and compaction lead to the formation of the final banded iron formation (BIF); (5) secondary enrichment by weathering and leaching of some minerals after uplift and exposure to the Earth's surface. Quartz dominates the mineral assemblages of the BIF, constituting about 53 wt.%, followed by the iron oxides, averaging about 44 wt.%. Other minerals such as carbonates and silicates occur in minor concentrations with a total of less than 3 wt.%. The majority of quartz and iron oxides are the primary precipitates' recrystallization products (cryptocrystalline chert, primary hematite, and magnetite). The carbonate fraction and iron silicates were commonly replaced by silica or iron oxides.

Funding *The project is funded by the Goven Mbeki Research and Development Center (GMRDC), University of Fort Hare, South Africa.*

References

- [1] Bekker A, Slack JF, Plnavsky N, Hoffman A, Konhauser KO, and Rouxel OJ. Iron formation: The sedimentary product of a complex interplay among mantle, tectonic, oceanic, and biospheric processes *Econ Geol*, 2010; 105: 467–508.
- [2] Eggseder M, Cruden AR, Tomkins AG, Wilson SA, Langendam AD. Colloidal origin of microbands in banded iron formations *Geochemical perspectives letters*, 2018;6: 43–49.
- [3] Eggseder MS, Cruden AR, Tomkins AG, Wilson SA, Dalstra HJ, Rielli A, Faivre D. Tiny particles building huge ore deposits—particle-based crystallisation in banded iron formation-hosted iron ore deposits (Hamersley Province, Australia) *Ore Geology Reviews*, 2019; 104: 160–174.
- [4] Dodd MS, Papineau D, She ZB, Manikyamba C, Wan YS, O'Neil J, Pirajno F. Widespread occurrences of variably crystalline ¹³C-depleted graphitic carbon in banded iron formations *Earth and Planetary Science Letters*, 2019; 512: 163–174.
- [5] Bekker A, Holland HD, Wang PL, Rumble D, Stein HJ, Hannah JL, Coetzee LL, Beukes, NJ Dating the rise of atmospheric oxygen, *Nature*, 2004; 427: 117–120.
- [6] Gross GA. A classification of iron formations based on depositional environments *Can Mineral*, 1980; 18: 215–222.
- [7] Gutzmer J, Chisonga BC, Beukes, NJ. The geochemistry of banded iron formation-hosted high-grade hematite-martite iron ores In: Hagemann, S, Rosière, C, Gutzmer, J and Beukes, NJ (Eds), *Reviews in Economic Geology*, 2008; 15: 157–183.
- [8] Haugaard R, Pecoits E, Lalonde S, Rouxel O, Konhauser K. The Joffre banded iron formation, Hamersley Group, Western Australia: Assessing the palaeoenvironment through detailed petrology and chemostratigraphy *Precambrian Research*, 2016; 273: 12–37.
- [9] James HL. Sedimentary facies of iron-formation *Economic Geology*, 1985; 49: 235–293.
- [10] Simonson BM. Sedimentological constraints on the origins of Precambrian iron-formations *Geological Society of America Bulletin*, 1985; 96(2): 244–252.
- [11] Trendall AF, Blockley JG. The iron formations of the Precambrian Hamersley Group, Western Australia, with special reference to the associated crocidolite *Geological Survey of Western Australia Bulletin*, 1970; 119: 328–353.
- [12] Chan MA, Johnson CM, Beard BL, Bowman JR, Parry WT. Iron isotopes constrain the pathways and formation mechanisms of terrestrial oxide concretions: A tool for tracing iron cycling on Mars? *Geosphere*, 2006; 2(7): 324–332.
- [13] Rasmussen B, Muhling JR, Suvorova A, Krapež B. Dust to dust: Evidence for the formation of "primary" hematite dust in banded iron formations via oxidation of iron silicate nanoparticles *Precambrian Research*, 2016; 284: 49–63.
- [14] Baidya AS, Pal DC, and Upadhyay D. Chemical weathering of garnet in Banded Iron Formation: Implications for the mechanism and sequence of secondary mineral formation and mobility of elements *Geochimica et Cosmochimica Acta*, 2019; 265: 198–220.

- [15] Johnson CM, Beard B L, Klein C, Beukes NJ, Roden EE. Iron isotopes constrain biologic and abiologic processes in banded iron formation genesis *Geochimica et Cosmochimica Acta*, 2008; 72(1): 151–169.
- [16] Klein C. Some Precambrian banded iron-formations (BIFs) from around the world: Their age, geologic setting, mineralogy, metamorphism, geochemistry, and origin *American Mineralogist*, 2005; 90: 1473–1499.
- [17] Klein C, Beukes NJ. Time distribution, stratigraphy, and sedimentologic setting, and geochemistry of Precambrian iron formations In: Schopf, JW, and Klein, C, eds, *The Proterozoic biosphere*: Cambridge, Cambridge University Press 1992, 139–146.
- [18] Klein C, Ladeira EA. Petrography and geochemistry of the least altered banded iron-formation of the Archean Carajás Formation, northern Brazil *Economic Geology*, 2002; 97(3) : 643–651.
- [19] Pickard AL, Barley ME, Krapež B. Deep-marine depositional setting of banded iron formation: sedimentological evidence from interbedded clastic sedimentary rocks in the early Palaeoproterozoic Dales Gorge Member of Western Australia *Sedimentary Geology*, 2004; 170(2): 37–62.
- [20] Trendall AF. The significance of iron-formation in the Precambrian stratigraphic record In: Altermann, W, Corcoran, PL (eds) *Precambrian Sedimentary Environments: A Modern Approach to Depositional Systems*. International Association of Sedimentologists Special Publication, Blackwell, Oxford 2002, 33: 33–66.
- [21] Kulik DA, Korzhnev MN. Lithological and geochemical evidence of Fe and Mn pathways during deposition of Lower Proterozoic banded iron formation in the Krivoy Rog basin (Ukraine). *Geological Society, London, Special Publications*, 1997; 119(1): 43–80.
- [22] Morris RC (1983). Supergene alteration of banded iron-formation In *Developments in Precambrian geology*, 6: 513–534.
- [23] Lascelles DF. Banded iron formation to high-grade iron ore: a critical review of supergene enrichment models *Australian Journal of Earth Sciences*, 2012; 59(8): 1105–1125.
- [24] Maynard JB. *Manganese In Geochemistry of Sedimentary Ore Deposits*, Springer, New York 1983, 121–145.
- [25] Schneiderhan EA, Gutzmer J, Strauss H, Mezger K, Beukes NJ. The chemostratigraphy of a Paleoproterozoic MnF-BIF succession—the Voelwater Subgroup of the Transvaal Supergroup in Griqualand West, South Africa *South African Journal of Geology*, 2006; 109(2): 63–80.
- [26] Spier CA, de Oliveira SM, Sial AN, Rios FJ. Geochemistry and genesis of the banded iron formations of the Cauê Formation, Quadrilátero Ferrífero, Minas Gerais, Brazil *Precambrian Research*, 2007; 152(3): 170–206.
- [27] Beukes NJ. Lithofacies and stratigraphy of the Kuruman and Griquatown Iron Formations, Northern Cape Province, South Africa *Trans Geol Soc S Afr*, 1980; 83:69–86.
- [28] Beukes NJ. Palaeoenvironmental setting of iron-formations in the depositional basin of the Transvaal Supergroup, South Africa, In: *Iron-Formation, facts and problems*, *Developments in Precambrian Geology*, 1983; 6: 131–209.
- [29] Beukes NJ. Sedimentology of the Kuruman and Griquatown iron-formations, Transvaal Supergroup, Griqualand West, South Africa: *Prec Res*, 1984; 24: 47–84.
- [30] Button A. The Transvaal sub-basin of the Transvaal Sequence, in: *Mineral Deposits of Southern Africa*, eds, CR Anhaeusser and S Maske: *Geol Soc S Afr*, 1986; 6: 811–817.
- [31] Cornell DH, Schutte SS, Eglinton BL. The Ongeluk basaltic andesite formation in Griqualand West, South Africa: Submarine alteration in 2222Ma Proterozoic sea *Precambrian Research*, 1996; 79: 101–124.
- [32] Eriksson PG, Schweitzer JK, Bosch PJA, Schreiber UM, van Deventer JL, Hatton CJ. The Transvaal sequence: an overview *Journal of African Earth Sciences (and the Middle East)*, 1993; 16(2): 25–51.
- [33] Miyano T, Beukes NJ. Phase relations of stilpnomelane, ferri-annite, and riebeckite in very low-grade metamorphosed iron-formations *Trans Geol Soc S Afr*, 1984; 87: 111–124.
- [34] Miyano T, Beukes NJ. Physicochemical Environments or the Formation of Quartz-Free Manganese Oxide Ores from the Early Proterozoic Hotazel Formation, Kalahari Manganese Field, South Africa, *Economic Geology*, 1987; 82, 706–718.
- [35] Moore JM, Tsikos H, Polteau S. Deconstructing the Transvaal Supergroup, South Africa: Implication for Palaeoproterozoic palaeoclimate models *Journal of African Earth Sciences*, 2001; 33: 437–444.
- [36] Beukes NJ. The Transvaal Sequence in the Griqualand West, In: CR, Anhaeusser, and S, Maske, (Eds), *Mineral Deposits of Southern African*, *Geological Society of South Africa*, 1986; 819–828.
- [37] Beukes NJ, Gutzmer J. Origin and paleoenvironmental significance of major iron formations at the Archean-Paleoproterozoic boundary, in Hagemann S, et al, eds, *Banded iron formation-*

- related high-grade iron ore: Society of Economic Geologists Reviews in Economic Geology, 2008; 15:5–47.
- [38] Grobbelaar WS, Burger MA, Pretorius AI, Marais W, van Niekerk IJ. Stratigraphic and structural setting of the Griqualand West and the Olifantshoek Sequences at Black Rock, Beeshoek and Rooinekke Mines, Griqualand West, South Africa Mineralium Deposita, 1995; 30: 152–161.
- [39] Horstmann UE, Halbich IW. Chemical composition of banded iron-formations of the Griqualand West Sequence, Northern Cape Province, South Africa, in comparison with other Precambrian iron-formations: Prec Res, 1995; 72: 109–145.
- [40] Knoll AH, Beukes NJ. Introduction: Initial investigations of a Neoproterozoic shelf margin-basin transition (Transvaal Supergroup, South Africa), Precambrian Research, 2009; 169: 1–14.
- [41] Altermann W, Halbich IW. Structural history of the south-western corner of the Kaapvaal Craton and the adjacent Namaqua realm: new observations and reappraisal Precambrian Research, 1991; 52: 133–166.
- [42] Beukes NJ. Facies relations, depositional environments and diagenesis in a major early proterozoic stromatolitic carbonate platform to basinal sequence, Campbellrand Subgroup, Transvaal Supergroup, Southern Africa Sedimentary Geology, 1987; 54, 21–46.
- [43] Beukes NJ, Klein C. Geochemistry and sedimentology of a Facies transition from microbanded to granular iron-formation in the early Proterozoic Transvaal Supergroup, South Africa: Precambrian Research, 1980; 47: 99–119.
- [44] Stowe CW. Synthesis and interpretation of structures along the north-eastern boundary of the Namaqua tectonic province, South Africa Transactions of the Geological Society of South Africa, 1986; 89: 185–198.
- [45] Cheney ES. Sequence stratigraphy and plate tectonic significance of the Transvaal succession of Southern Africa and its equivalent in Western Australia, Precambrian Research, 1996; 79: 3–24.
- [46] Nel BP. Petrography and Geochemistry of Iron Formations of the Paleoproterozoic Koegas Subgroup, Transvaal Supergroup, Griqualand West, South Africa MSc thesis (unpublished), University of Johannesburg 2013, 71–104.
- [47] Angerer T, Hagemann SG, Danyushevsky LV. Geochemical evolution of the banded iron formation-hosted high-grade iron ore system in the Koolyanobbing Greenstone Belt, Western Australia Economic Geology, 2012; 107: 599–644.
- [48] Klein C, Ladeira EA. Geochemistry and mineralogy of Neoproterozoic banded iron-formations and some selected, siliceous manganese formations from the Urucum District, Mato Grosso do Sul, Brazil Economic Geology, 2004; 99(6): 1233–1244.
- [49] Morris RC. A textural and mineralogical study of the relationship of iron ore to banded iron-formation in the Hamersley iron province of Western Australia Economic Geology, 1980; 75(2): 184–209.
- [50] Walker JC. Suboxic diagenesis in banded iron formations. Nature, 1984; 309: 340–342.
- [51] Bland W, Rolls D. Weathering An Introduction to the Scientific Principles – Arnold Publishers, London 1998; 45–67.
- [52] Ghosh D, Dutta T, Samanta SK, Pal DC. Texture, microstructure and geochemistry of magnetite from the Banduhurang uranium mine, Singhbhum Shear Zone, India—implications for physico-chemical evolution of magnetite mineralisation Journal of the Geological Society of India, 2013; 81(1): 101–112.
- [53] Colombo U, Gazzarrini F, Lanzavecchia G, Sironi G. Magnetite oxidation: A proposed mechanism Science, 1965; 147: 1033–1043.
- [54] Fisher RS, Land LS. Diagenetic history of Eocene Wilcox sandstones, south-central Texas Geochimica et Cosmochimica Acta, 1986; 50(4): 551–561.
- [55] Dutton SP, Land LS. Meteoric burial diagenesis of Pennsylvanian arkosic sandstones, south-western Anadarko Basin, Texas AAPG bulletin, 1985; 69(1): 22–38.
- [56] Trendall AF. The significance of iron-formation in the Precambrian stratigraphic record. In: Altermann, W., Corcoran, P.L. (eds.) Precambrian Sedimentary Environments: A Modern Approach to Depositional Systems, 2002; volume. 33. International Association of Sedimentologists Special Publication, Blackwell, Oxford, 33–66.
- [57] Eriksson PG, Altermann W, Hartzer FJ. The transvaal supergroup and precursors In: Johnson, MR, Annhaeusser, CR Thomas, RJ (Eds) The Geology of South Africa Geol Society of South Africa, 2006; 237–260.

To whom correspondence should be addressed: professor Dr. Christopher Baiyegunhi, Department of Geology and Mining, University of Limpopo, Private Bag X1106, Sovenga 0727, Limpopo Province, South Africa, E-mail: christopher.baiyegunhi@ul.ac.za